Multi-tissue network analysis reveals the effect of JNK inhibition on dietary sucrose-induced metabolic dysfunction in rats

Hong Yang[1], Cheng Zhang[1], Woonghee Kim[1], Mengnan Shi[1], Metin Kiliclioglu[2], Cemil Bayram[3], Ismail Bolat[2], Özlem Özdemir Tozlu[4], Cem Baba[4], Nursena Yuksel[4], Serkan Yildirim[2], Shazia Iqbal[5], Jihad Sebhaoui[5], Ahmet Hacımuftuoglu[3], Mathias Uhlen[1], Jan Boren[6], Hasan Turkez[7], Adil Mardinoglu[1,8, *, $]

[1]Science for Life Laboratory, KTH - Royal Institute of Technology, Stockholm, Sweden

[2]Department of Pathology, Veterinary Faculty, Atatürk University, Erzurum, 25240, Turkiye

[3]Department of Medical Pharmacology, Faculty of Medicine, Atatürk University, 25240, Erzurum, Turkiye.

[4]Department of Molecular Biology and Genetics, Faculty of Science, Erzurum Technical University, 25200 Erzurum, Turkiye.

[5]Trustlife Labs Drug Research & Development Center, 34774 Istanbul, Turkiye.

[6]Department of Molecular and Clinical Medicine, University of Gothenburg, Sahlgrenska University Hospital, Gothenburg, Sweden

[7]Department of Medical Biology, Faculty of Medicine, Atatürk University, Erzurum, Turkiye

[8]Centre for Host-Microbiome Interactions, Faculty of Dentistry, Oral & Craniofacial Sciences, King's College London, London, SE1 9RT, United Kingdom

*Corresponding author: adilm@scilifelab.se (Adil Mardinoglu)

[$] Lead contact.

Abstract

Excessive consumption of sucrose, in the form of sugar-sweetened beverages, has been implicated in the pathogenesis of metabolic dysfunction-associated fatty liver disease (MAFLD) and other related metabolic syndromes. The c-Jun N-terminal kinase (JNK) pathway plays a crucial role in response to dietary stressors, and it was demonstrated that the inhibition of the JNK pathway could potentially be used in the treatment of MAFLD. However, the intricate mechanisms underlying these interventions remain incompletely understood given their multifaceted effects across multiple tissues. In this study, we challenged rats with sucrose-sweetened water and investigated the potential effects of JNK inhibition by employing network analysis based on the transcriptome profiling obtained from hepatic and extrahepatic tissues, including visceral white adipose tissue, skeletal muscle, and brain. Our data demonstrate that JNK inhibition by JNK-IN-5A effectively reduces the circulating triglyceride accumulation and inflammation in rats subjected to sucrose consumption. Coexpression analysis and genome-scale metabolic modelling reveal that sucrose overconsumption primarily induces transcriptional dysfunction related to fatty acid and oxidative metabolism in the liver and adipose tissues, which are largely rectified after JNK inhibition at a clinically relevant dose. Skeletal muscle exhibited minimal transcriptional changes to sucrose overconsumption but underwent substantial metabolic adaptation following the JNK inhibition. Overall, our data provides novel insights into the molecular basis by which JNK inhibition exerts its metabolic effect in the metabolically active tissues. Furthermore, our findings underpin the critical role of extrahepatic metabolism in the development of diet-induced steatosis, offering valuable guidance for future studies focused on JNK-targeting for effective treatment of MAFLD.

Keywords: MAFLD, JNK, Sucrose, JNK-IN-5A, multi-tissue transcriptome

Introduction

Hepatic steatosis (HS) is characterized by the accumulation of triglycerides (TG) in the liver (at least 5% of liver weight) in the absence of secondary contributing factors (Nassir et al., 2015). Metabolic dysfunction-associated fatty liver disease (MAFLD) encompasses a spectrum of conditions, ranging from simple HS to nonalcoholic steatohepatitis (NASH), which is characterized by HS combined with various degrees of liver inflammation and liver injury, with or without fibrosis. NASH can progress to advanced liver disease including cirrhosis and hepatocellular carcinoma (Machado and Cortez-Pinto, 2023). The global prevalence of MAFLD is estimated to be 20~25% (Younossi et al., 2023), and it is rapidly increasing in parallel with the epidemic of obesity and type 2 diabetes mellitus (Kotsiliti, 2023; Le et al., 2023). Given the absence of approved pharmacological therapy for MAFLD by the US Food and Drug Treatment (FDA) (Llovet et al., 2023; Nassir et al., 2015), the discovery and development of effective therapies are of great importance in MAFLD treatment.

The progression of MAFLD is associated with various factors, including overnutrition, genetic determinants, and associated comorbidities (Sveinbjornsson et al., 2022; Yki-Jarvinen et al., 2021). Strong evidence from meta-analysis, prospective cohort studies, and observational studies indicate that excessive sucrose, a disaccharide that comprises equal amounts of glucose and fructose and is prevalent in all kinds of sugar-sweetened beverages, maybe an initial factor for the development of MAFLD (Geidl-Flueck et al., 2021; Geurtsen et al., 2021; Karlsen et al., 2022; Malik and Hu, 2022; Zhang et al., 2021). For instance, a previous study reported that rats subjected to a 12-week high-sucrose diet (25% w/v sucrose), developed a metabolic syndrome phenotype characterized by glucose intolerance, HS, and insulin resistance (IR) (Sousa et al., 2018). Recent research further reveals that the consumption of sucrose at a concentration of 10% w/v can disrupt energy balance and induce

HS within 10-20 weeks (Jang et al., 2020; Stephenson et al., 2022). In this context, c-Jun-N-terminal Kinase (JNK), a mitogen-activated protein kinase family member, emerges as a critical player due to its known function in response to intra- and extracellular stress, including hypercaloric diet consumption (Nikolic et al., 2020; Sabio et al., 2009; Softic et al., 2020). Indeed, accumulating evidence implicated JNK in the pathogenesis of diet-induced obesity, IR, development of metabolic syndrome and MAFLD (Czaja, 2010; Sabio and Davis, 2010; Seki et al., 2012; Singh et al., 2009). JNK has three isoforms: JNK1 and JNK2, which are ubiquitously expressed, and JNK3 is specifically expressed in the brain, testis and heart (Chang and Karin, 2001). Previously, Singh et al. demonstrated that increased hepatic JNK signalling occurred simultaneously with steatosis and lipid accumulation in a steatohepatitis model induced by a methionine- and choline-deficient diet (MCD) (Singh et al., 2009). Notably, MCD diet-fed JNK1 null mice exhibited significantly reduced levels of key hallmarks of MAFLD, including HS, TG accumulation, inflammation, lipid peroxidation, hepatocyte injury, and apoptosis (Singh et al., 2009). Similarly, high-fat diet-fed mice with hepatic ablation of both JNK1 and JNK2 are protected from HS and IR (Vernia et al., 2014). Altogether, these findings suggest that the suppression of the JNK pathway may prevent the development of HS and related metabolic syndrome (Kodama and Brenner, 2009; Schattenberg et al., 2006). However, whether JNK mediates the metabolic disruption induced by sucrose overconsumption remains to be elucidated. Moreover, our previous study demonstrated that JNK-IN-5A, a selective JNK2 and JNK3 inhibitor (Angell et al., 2007; Cerbone et al., 2012), effectively decreased fat accumulation and steatosis-related protein expression in an *in vitro* steatosis model (Kim et al., 2023). However, the inhibitory effect of JNK-IN-5A to JNK and JNK-related pathways in *in vivo* is unknown. It is established that JNK exerts its metabolic regulation as a result of multi-tissue communication, including those between liver and adipose tissues (Azzu et al., 2020), and skeletal muscle (Nikolic et al.,

2020; Vernia et al., 2014). A systematic investigation into tissue-specific and tissue-crosstalk metabolic changes in response to diet and therapy interventions is, therefore, paramount by using genome-scale metabolic models (GEMs). GEMs are the collection of biochemical reactions and the associated enzymes and transporters between the cellular compartments and such models can be used in the analysis of omics data for gaining insights and interpretation of the omics data (Mardinoglu et al., 2013; Mardinoglu et al., 2018; Mardinoglu and Nielsen, 2012).

In this study, we first performed a 7-day oral toxicology study and studied the tolerability of JNK-IN-5A in rats. Next, we explored the potential therapeutic effect of JNK-IN-5A under high sucrose consumption in *in vivo* by performing systems biology analysis. To elucidate the systems-wide impact of sucrose overconsumption and JNK-IN-5A treatment, we investigated the intra- and inter-tissue response through integrative analysis of transcriptomics profiles from the metabolically active tissues, including liver and three other extrahepatic tissues, including visceral white adipose tissue (vWAT), skeletal muscle (SkM) and brain tissues. We further predicted the genome-wide metabolic activity changes induced by liquid sucrose ingestion and JNK-IN-5A treatment by performing genome-scale metabolic modelling.

Results

The acute effect of the JNK-IN-5A in rats

We previously showed that the JNK-IN-5A can effectively decrease the TG accumulation and steatosis-related protein levels in an *in vitro* model simulating the activated *de novo* lipogenesis in MAFLD patients (Kim et al., 2023). Here, we first performed a 7-day oral toxicology study and studied the tolerability of JNK-IN-5A in rats. Four groups of three males and three females were given vehicle and doses of 30, 100 and 300 mg/kg of JNK-IN-

5A, once a day for 7 days (**Fig. 1, Fig, 2a**). We assessed clinical adverse effects, body weight, and clinical pathological parameters during the study.

A few animals including those given vehicles displayed noisy respiration and reflux. These signs were only observed in connection with dosing, suggesting to be related to the high viscosity of the formulation and foul taste, and are not considered as systemic side effects of the JNK-IN-5A administration. We observed none of the administrated doses led to significant changes in body weight and haematological parameters (**Data S1**). Clinical chemistry parameters revealed lower plasma levels of glucose, blood urea nitrogen and total proteins in female rats given JNK-IN-5A at all three doses (**Fig. 2a, Data S1**). In addition, the two higher doses of JNK-IN-5A decreased the levels of sodium in female rats and elevated the level of phosphate in both sexes (**Fig. 2a, Data S1**). Overall, the administration of JNK-IN-5A is well tolerated with regard to adverse clinical signs, body weight and clinical haematology parameters.

Treatment of liquid sucrose-induced fatty liver with JNK-IN-5A

We next investigated the effect of JNK-IN-5A treatment in a rat model of MAFLD induced by liquid sucrose ingestion (**Fig. 1b**). The rats feeding a standard chow diet received either tap water (control group) or sucrose-containing water (10% w/v sucrose, sucrose group) for 4 weeks, after which rats on sucrose watering were further divided into subgroups: sucrose only group and JNK-IN-5A-treated groups at a regular dosage of 30 mg/kg/day (sucrose+JNK_D1 group) or a higher dosage of 60 mg/kg/day (sucrose+JNK_D2 group), for 3-weeks. A total of 44 rats were used in this study (n = 11 rats per group).

We observed that liquid sucrose consumption resulted in significantly increased plasma levels of TG ($p < 0.0001$) and lactate dehydrogenase (LDH, $p < 0.0001$), which is an inflammation marker, compared to the healthy controls (**Fig. 2b, Data S2**). On sucrose water,

JNK-IN-5A-treated rats exhibited significantly lower levels of TG (JNK_D1, $p < 0.0001$; JNK_D2, $p < 0.001$), aspartate aminotransferase (AST; JNK_D1, $p = 0.09$; JNK_D2, $p = 0.005$), and LDH (JNK_D1, *n.s.*; JNK_D2, p = 0.015) but had no significant change on body weight, glucose, high-density lipoprotein (HDL) and low-density lipoprotein (LDL) as compared to their corresponding controls (**Fig. 2b, Data S2**). We also performed neurological tests to study the potential effect of JNK-IN-5A on the brain. We found that there is no significant difference between the groups in terms of learning and memory abilities assessed by the passive avoidance test (**Data S3**). Furthermore, the locomotor activity test (**Data S4**) and elevated plus maze test (**Data S5**) collectively indicate the JNK-IN-5A-treated rats exhibit no evidence of anxiety and behaviour disorders.

To investigate the gene-level inhibition of JNK upon JNK-IN-5A treatment, we further examined the mRNA expression of JNK1 (encoded by the gene *Mapk8*), JNK2 (encoded by the gene *Mapk9*) and JNK3 (encoded by the gene *Mapk10*) in the study. As anticipated, *Mapk8* and *Mapk9* have high expression in all these tissues (liver, vWAT, SkM, and brain) whereas *Mapk10* is highly expressed specifically in the brain tissue (**Fig. 2c, Fig. S1a**). Our analysis indicates that the treatment of JNK_D1 effectively alleviated the JNK1 gene expression in the liver (*padj* = 0.03) and exerted more profound inhibitory effects on both JNK1 (*padj* = 0.0009) and JNK2 gene expression (*padj* = 2.2e-07) in SkM (**Fig. 2c, Data S6**). Interestingly, we found that plasma TG level is significantly correlated with the JNK2 gene expression in SkM (**Fig. 2d&e**). In brain tissue, we found JNK3 gene expression exhibited a trend of dose-dependently inhibition in the JNK-IN-5A-treated groups. Particularly, the downregulation of JNK3 in the sucrose+JNK_D2 group approaches the borderline of significance (*padj* = 0.07), compared to those, which drank sweetened water group only (sucrose group) (**Data S6**).

JNK inhibition rewires metabolic perturbation in the liver and vWAT

To gain in-depth insight into system-level transcriptional response to sucrose consumption and JNK-IN-5A treatment, we next studied the global gene expression profiles in both liver and extrahepatic tissues (vWAT, SkM, and brain). A total of 19,780 protein-coding genes in the rat genome were analyzed (Martin et al., 2023). Principal component analysis (PCA) revealed that liquid sucrose ingestion resulted in the largest transcriptional changes in the liver and vWAT (**Fig. 3a**), which is consistent with previous results (Stephenson et al., 2022). Of note, we observed that JNK-IN-5A treatment, especially JNK_D1, corrected to a large extent of the gene expression profile in the liver and vWAT of treated-rats towards the profile of healthy controls on a principal components space (**Fig. 3a**). In SkM, the transcriptional difference is primally driven by JNK_D1 treatment and showed a clear separation (**Fig. 3a**).

In parallel with the results presented above, differential gene expression analysis revealed that the liver had the largest number of differentially expressed genes (DEGs, DESeq2-Benjamini-Hochberg adjusted $p < 0.01$) associated with liquid sucrose ingestion, comprising a total of 2,771 DEGs (14%), followed closely by vWAT with 2,724 DEGs (13.8%), SkM with 257 DEGs (1.3%), and the brain with a modest 30 DEGs (0.2%) (**Fig. 3b&c**, **Fig. S1b-e, Data S6**). Moreover, we observed that JNK_D1 treatment demonstrated a remarkable effect in the reversal of gene expression patterns related to sucrose consumption. Specifically, in the liver, JNK_D1 treatment substantially suppressed the expression of 60.7% (1,143 out of 1,884, hypergeometric $p \approx 0$) sucrose-induced DEGs and elevated the expression of 22% of sucrose-repressed genes (195 out of 887, hypergeometric p = 6.9e-129) (**Fig. 3d**, **Fig. S1b**). Likewise, we observed a reversal of 42.2% and 31.4% (698 of 1,655 and 336 out of 1,069, respectively) DEGs in vWAT (**Fig. 3d**, **Fig. S1c**). It should be noted that, in both liver and vWAT, the effect of JNK_D2 treatment is relatively smaller than JNK_D1 in terms of the corrections of DEGs (**Fig. S2a&b**). Pathway enrichment analysis of JNK_D1 reversed genes identified significantly enriched KEGG pathways related to carbon metabolism, fatty acid

metabolism, protein processing in ER, and oxidative phosphorylation (OXPHOS) (Benjamini-Hochberg adjusted $p < 0.01$) (**Fig. S2c&d**). Interestingly, some of the genes exhibited opposing regulation in the liver and vWAT in response to the interventions of sucrose only and the combination of sucrose intervention and JNK-IN-5A treatment. This is exemplified in genes related to fatty acid degradation, elongation and biosynthesis (up in the liver and down in vWAT in sucrose only group, while down in the liver and up in vWAT in sucrose plus JNK-IN-5A-treated groups), including *Cpt2*, *Acads*, *Acadvl*, *Acat1*, *Acot5*, *Eci3*, *Hsd17b12*, and *Oxsm* (**Fig. S3, Data S6**); genes related to fatty acid (FA) uptake, including fatty acid binding proteins *Fabp1*, *Fabp4* and transporters *Slc27a1* and *Slc27a5* (**Fig. S4, Data S6**); and genes related to redox homeostasis, including *Prdx4*, a secreted enzyme that scavenges redox oxidative stress (ROS), *Selenos*, and *Ndufa6* (**Fig. S5, Data S6**). Taken together, these results suggest that JNK-IN-5A treatment reshapes sucrose-induced transcriptional changes in both the liver and vWAT, reinforcing their metabolic synergy in FA uptake and metabolism (Stephenson et al., 2022).

JNK inhibition in SkM correlated with the regulation of energy metabolism in the liver and vWAT

It has been reported that JNK acts as a critical mediator of muscle phenotype and adaptive remodelling in animals and humans (Lessard et al., 2018). Here, we found that in contrast to the massive transcriptional regulation observed in the liver and vWAT, liquid sucrose intake has minimal impact on SkM in terms of both genome-wide transcriptional variance (**Fig. 3a**) and the number of DEGs (**Fig. 3a, Fig. 4a&b)**. While in JNK_D1-treated SkM, a substantial quantitative difference in gene expression emerged, encompassing 4,159 (20.9%) DEGs, of which 97% up-regulated (1,552 out of 1,588) and 99% down-regulated (2,557 out of 2,571) genes being exclusively dependent on the JNK_D1 treatment (**Fig. 4a&b**). Functional analysis revealed that many of the upregulated genes are involved in immune-related

pathways, including hematopoietic cell lineage (HSCs), osteoclast differentiation, chemokine signalling pathway, phagosome, and Fc gamma R-mediated phagocytosis, and down-regulated genes are involved in OXPHOS, thermogenesis, TCA cycle, carbon metabolism, cardiac muscle contraction, and insulin signalling pathway (**Fig. 4c&d, Fig. 5**). Among the genes regulated by both sucrose-feeding and JNK_D1 treatment in SkM were those involved in the insulin signalling pathway (e.g., *Ppp1r3f, Phkg1, Phkb*) (**Fig. 5**). As this intra-tissue effect was observed in JNK_D1 not in the JNK_D2-treated group (**Fig. 3b, Fig. S5a**), we subsequently investigated the inter-tissue regulation based on the significantly transcriptional changes (as indicated by the $\log_2$-Fold change, $\log_2$FC) in response to JNK_D1 treatment and found that $\log_2$FC of shared DEGs between JNK_D1-treated SkM and liver, vWAT or brain exhibited strong agreements (**Fig. 4e, Fig S5b**). Specifically, 86% and 69% of shared DEGs between SkM and vWAT, and the brain, exhibited consistent changes in response to JNK_D1 treatment (the same $\log_2$FC sign, indicating either upregulated or downregulated in both tissues being compared), with a Spearman correlation of 0.78 and 0.54, respectively. These shared DEGs were found to be involved in several critical metabolic processes, including cholesterol metabolism, bile acid biosynthesis and secretion (such as *Lipc*, *Apob*, *Slc7a1*, *Angptl3*, *Slc10a1*), and regulation of energy homeostasis (e.g., *Lep*), suggesting that SkM had a major metabolic adaptation to JNK_D1 treatment and exerts its metabolic effect, at least partially, through coordinated interactions with other tissues.

Inter-tissue network analysis revealed the JNK-IN-5A inhibition-associated molecular mechanism

To better understand the regulation of lipid metabolism and energy homeostasis at a system-wide level in an unbiased manner, we next performed gene co-expression network (GCN) analysis to study intra- and inter-tissue coordination of metabolic pathways as well as biological processes that are associated with sucrose-feeding and/or JNK_D1 inhibition.

GCN, a robust systems biology approach (Barabasi and Albert, 1999), allows us to study the functionality of the gene module and its constituent genes. These genes are more likely to be co-expressed if they are either regulated by the same transcription factors or share similar topological properties in protein-protein interaction networks (Califano et al., 2012; Dobrin et al., 2009; Zhang et al., 2016). By investigating the importance and topology of these functional modules, it is possible to understand the biological mechanisms underpinning the disease and/or therapy intervention (Choobdar et al., 2019; Yang et al., 2021; Yang et al., 2014).

We first constructed tissue-specific GCN based on the whole transcriptomics data and selected highly connected genes from the network (the top 10% positively correlated genes that fulfilled FDR < 0.05), followed by module detection using the Leiden clustering algorithm (**Fig. S7a; Data S7**). We subsequently evaluated the enrichment of DEGs in the modules to identify those associated with sucrose consumption, JNK_D1 treatment, or both (so-called perturbated module). As expected, GCN analysis revealed distinct gene expression patterns across different tissues (**Fig. 6a**). For instance, in module 1 in the liver (Liver.M1), vWAT.M4, SkM.M4, and Brain.M4, we found a significant enrichment of genes that exhibited elevated expression in response to sucrose consumption while simultaneously being suppressed by JNK_D1. Conversely, Liver.M0 and vWAT.M3 exhibited significant enrichment of genes repressed by sucrose intake but elevated after JNK_D1 treatment. These distinct expression patterns collectively reflect the combined metabolic effect of sucrose-feeding and JNK_D1 interventions. Additionally, GCN analysis identified modules associated with either sucrose-feeding or JNK_D1 intervention at the tissue level, for example, vWAT.M0 (sucrose), vWAT.M1 and Brain.M5 (JNK_D1) (**Fig. 6a**).

To pinpoint gene modules involved in inter-tissue communication, we conducted a correlation analysis among inter-tissue modules using their module eigengene (**see details in**

Method) and assessed the enrichment of genes from these modules in MSigDB hallmark gene sets. Our analysis revealed a significant correlation between SkM.M0 and Liver.M0 (R = 0.67, $padj$ = 0.006) as well as vWAT.M3 (R = 0.58, $padj$ = 0.03) (**Fig. 6b&c**). This correlation aligns with the functional annotation of genes within these modules, including those associated with mTORC1 signalling, PI3K/AKT/mTOR signalling, DNA Repair, and unfolded protein response (**Fig. 6d**). Interestingly, we observed that *Mapk9* is among the module members of SkM.M0, indicating a potential metabolic link coordinated by JNK inhibition, connecting SkM with other tissues, including the liver and vWAT (**Fig. 6b**, **Data S7**). SkM.M1 and Liver.M2 (R = -0.66, $padj$ = 0.006), SkM.M3 and vWAT.M0 (R = 0.60, $padj$ = 0.03), and SkM.M4 and vWAT.M3 (R = -0.66, $padj$ = 0.006) were also found to be significantly correlated (R = -0.57, $padj$ = 0.03). Note that genes in Liver.M1, vWAT.M3, SkM.M0, SkM.M4, and Brain.M4 are commonly involved in adipogenesis, fatty acid metabolism, OXPHOS, and reactive oxygen species pathway (**Fig. 6d**). These observations suggest the potential crosstalk or regulatory relationship between these tissue modules after JNK_D1 treatment.

Metabolic modelling identified the metabolic reprogramming linked to JNK-IN-5A inhibition

To predict how tissue-level metabolic activity responds to sucrose feeding and JNK-IN-5A treatment, we performed an integrative analysis of transcriptomics data by generating tissue-specific GEMs and applying Compass (Wagner et al., 2021). Compass is a flux balance analysis-based (Orth et al., 2010) algorithms to model the metabolic state of a system (e.g., single cell or tissue), taking into account the observed expression levels of enzyme-coding genes in each sample from RNA-seq data. In this study, we employed Recon3D, a generic GEMs of human metabolism, comprising 10,600 metabolic reactions associated with 5,835 metabolites and 2,248 metabolic genes (Brunk et al., 2018). Consistent with our previous

analysis, we observed a shift in metabolic activity in the liver and vWAT after JNK_D1 treatment (**Fig. 7**, **Data S8**). Specifically, Compass predicted that 2,840 and 4,170 metabolic reactions showed significantly altered activity (Wilcoxon test, adjusted *p*-value < 0.05) following the sucrose consumption in the liver and vWAT, respectively. 89.2% and 88.3% of which were correspondingly reversed after JNK_D1 treatment (**Data S8**). The common altered reactions are partitions into the subsystems named citric acid cycle, fatty acid oxidation, fatty acid synthesis, and tryptophan metabolism in Recon3D (**Fig. 7c**). Interestingly, we found 8 metabolic reactions significantly altered in sucrose+JNK_D2-treated rats, including 2 reactions involved in glycolysis/gluconeogenesis, 2 in nucleotide interconversion, 1 in pentose phosphate pathway, 1 in fructose and mannose metabolism, 1 in propanoate metabolism (Cohen's d < 0, padj < 0.05), and 1 in drug metabolism (Cohen's d > 0, padj < 0.05) (**Data S8**). Hence our systems biology analysis revealed the molecular mechanisms altered due the JNK-IN-5A treatment.

Discussion

The aetiology of MAFLD is multifactorial and remains incompletely understood, impeding the progress in developing effective therapies for MAFLD. Our investigation into the metabolic changes from the major metabolically active tissues enabled us to systematically assess the potential therapeutic effects of JNK-IN-5A under high sucrose consumption. Here, we demonstrated that JNK-IN-5A attenuated the accumulation of circulating TG and inflammation exaggerated by liquid sucrose consumption. Importantly, the rats treated with JNK-IN-5A did not exhibit indications of anxiety or behavioural disorders. These results have important implications for the development of JNK3 inhibitors, taking into account the high expression of JNK3 in the brain (Chang and Karin, 2001). Additionally, our data indicated that JNK-IN-5A, a selective inhibitor of JNK2 and JNK3 (Angell et al., 2007; Cerbone et al., 2012), also exerted an inhibitory effect on the gene expression of JNK1 in *in*

vivo, especially in skeletal muscle (**Fig. 2**).

By studying the hepatic and extrahepatic tissues using genome-wide transcriptome data and integrative analyses with GEMs, we found that the intervention with sucrose-sweetened water triggered extensive transcriptional changes in the liver and adipose tissues, including those involved in fatty acid and oxidative metabolism. The metabolic axis between the liver and adipose tissues is a critical regulatory network that governs energy balance and metabolic homeostasis in the body (Azzu et al., 2020). It has been reported that upon chronic overnutrition, adipose lipogenesis is significantly downregulated, which leads to ectopic lipid accumulation and insulin resistance (Jeon et al., 2023). In line with this, we found that in the sucrose-sweetened water group, the mRNA expression of many genes related to fatty acid metabolism and uptake is downregulated in adipose tissue. Interestingly, those genes showed the opposite regulation between liver and adipose tissue, indicating their complementary role in these metabolic processes in response to the diet intervention. These findings also pinpoint the critical role of extrahepatic metabolism in the development of MAFLD.

JNK plays essential roles in a range of signalling pathways that have implications for metabolic processes such as insulin sensitivity, thermogenesis, adipogenesis, and lipid metabolism (Nikolic et al., 2020; Solinas and Becattini, 2017). Our data demonstrated that JNK-IN-5A, especially when administered at a regular dosage (JNK_D1, 30mg/kg/day), effectively opposite a substantial portion of the transcriptional changes induced by sucrose consumption, particularly those related to carbon, fatty acid metabolism, OXPHOS, and thermogenesis in the liver and adipose tissues. This suggests that JNK-IN-5A might hold promise as a potential strategy for restoring metabolic perturbation in tissues challenged by sucrose-induced stress. However, our study also revealed that JNK_D1-treated skeletal muscle exhibited profound transcriptional changes related to HSCs, osteoclast differentiation, and immune-related pathways. Importantly, we found that these changes were not isolated to

SkM but exhibited correlations with changes in liver, vWAT, and even brain tissue, evidenced by the correlation analysis and co-expression network analysis across tissues. Previously, Xiao *et al.* (Xiao et al., 2019) demonstrated that the JNK pathway regulates HSCs expansion and self-renewal in JNK-IN-8-treated $CD34^{+}$CD45RA-CB cells. Lessard *et al.* (Lessard et al., 2018) demonstrated that mice with muscle-specific JNK1/2 knockout, have a muscle phenotype that mimics that of endurance-trained athletes. Together with our data, these results suggest a multifaceted role of JNK signalling in the regulation of HSCs and metabolism in skeletal muscle. Further investigation is warranted to understand the precise mechanisms underlying these changes and their implications for skeletal muscle function and overall physiological homeostasis.

In summary, our study provides a comprehensive understanding of the therapeutic potential of JNK-IN-5A treatment in a rat model of sucrose-induced MAFLD. Through an analysis of genome-wide transcriptome data in the major metabolic tissues, we shed light on the JNK-IN-5A-mediated metabolic effects in both hepatic and extrahepatic tissues. This implies a potential therapeutic strategy for the treatment of diet-induced MAFLD and other metabolic complications, potentially by regulating cellular energy homeostasis and mitochondrial metabolism. Additional studies are needed to determine whether JNK inhibition can exert its therapeutic benefits in long-term dietary interventions, resembling the different stages of MAFLD, including the NASH model.

Materials and Methods

Experimental models and subject details

1. Oral Toxicity Study in Rats

Twelve male and twelve female rats of the Wistar strain (Envigo, Venray, Netherlands) were used to assess the 7-day oral (gavage) toxicology, in terms of clinical signs, body weight and clinical pathological parameters, of JNK-IN-5A in rats. Animals were group-housed under standard conditions and had free access to water and 2916C Teklad global 16 % protein rodent irradiated diet (Envigo, Venray, Netherlands). Dose levels of 0 (vehicle control), 30, 100, or 300 mg/kg of JNK-IN-5A were administered once daily via oral gavage for 7 days. The vehicle was 2 w/w% HPMC (Colorcon), 2 w/w% PS80 (Merck) in 10 mM PBS, pH 7 and dose volume was 5 mL/kg for JNK-IN-5A. Body weights were recorded the week before and within 24 hours before the start of dosing and on Day 3 and on necropsy Day 8. All animals were bled at 2 hours after dosing on Day 1 and Day 7. Blood samples were placed on ice after sample collection and centrifuged at approx. 3000xG, 5 min., 4°C. 7.5 µL plasma was transferred into a separate low-binding protein tube and the remaining plasma was transferred into a second low-binding tube. The tubes were frozen upright at approximately -20°C. Blood and plasma were analysed using an Exigo analyser and Vetscan equipment. The VetScan analyser was calibrated with calibration samples with known plasma levels of each parameter before the start of analysis, occasionally during the analysis period of study samples and after completed analyses. All the animal procedures (including housing, health monitoring, dosing, etc.) and ethical revisions were performed according to the 2010/63/EU Directive on the protection of animals used for biomedical research.

2. JNK-IN-5A Treatment Study in Rats

All experiments were performed in accordance with institutional ethical guidelines, and the present in vivo study was approved by the Ethics Committee for Animal Research of Atatürk University (with the reference number 2023/04 on 30.03.2023). Rats were obtained from the Atatürk University Experimental Research Center. All groups were housed on a 12-hour light and dark cycle. The temperature and humidity values of the environment were kept at optimal values. To prevent neophobia, rats were divided into groups one week before sucrose treatment by following the double-blind method to adapt to the laboratory environment and each other.

A total of 4 groups consisting of 11 subjects each were formed, including the healthy Control group consisting of rats received ad libitum tap water, the Sucrose group consisting of rats received ad libitum 10% Sucrose (BioShop, Canada, Lot No: 2E77269) (equivalent to the concentration of fructose in typical soda (Jang et al., 2020)), and groups treated by JNK-IN-5A at two concentration: sucrose+JNK_D1 group with rats received ad libitum 10% sucrose and 30 mg/kg/day JNK-IN-5A gavage and sucrose+JNK_D2 group with rats received ad libitum 10% sucrose and 60 mg/kg/day JNK-IN-5A gavage. The rats had ad libitum access to tap water (Control) or 10% sucrose water (sucrose, sucrose+JNK_D1, and sucrose+JNK_D2) and a standard chow diet throughout the experimental period. The amount of water consumed by all groups was recorded daily, and drinking water was renewed every day. After feeding with sucrose for 4 weeks, drug treatment was given at the following 3 weeks. Behavioural tests were taken before the experiment started and after 3 weeks of drug treatment. Locomotor activity tests, elevated plus maze tests and passive avoidance tests were used as behavioural tests. Behavioural tests were repeated at the end of the 21-day treatment regimen. While the last behavioural tests were being taken, drug treatment continued so that the drug level in the blood would not change. After the experimental animals were sacrificed with a

high dose (200 mg/kg thiopental sodium) anaesthetic, the relevant tissues were taken for further analysis.

2.1 Monitoring behaviour

All tests were performed twice in total, initially and after the 21-day treatment regimen. According to the results obtained from the initial measurements, rats with outliers for the experiment were determined. After the treatment measurement, it was determined whether there was any change in the behaviour of the rats. The **Locomotor Activity Test** is a system used to test differences in motor activity and anxiety-related behaviours of rats. In the system scanned with infrared rays, each of the ambulatory, stereotypical, rearings, resting percentage and travelled distance movements of the rats are digitized and converted to computer output. These outputs are evaluated and provide information that needs to be interpreted about the animal's adaptation to the new environment and the continuation of the sense of curiosity or anxiety. Stereotypical movement shows rats grooming and recognizing their environment. Ambulatory movement is all the movements that rats make on the ground without standing up. Distance shows the distance travelled by the rats in the cage. The rearing movement indicates the time the rats stand up in the cage. The resting percentage is an indicator of anxiety. Ambulatory movements are recorded with horizontal sensors that surround the cage 360 degrees at the base, and stereotypic and rearing movements are recorded with vertical sensors located 10 cm above the floor. The entire cage continues to be measured continuously with 250 ms infrared. Unlike the open field test, activity measurement is performed in this study and the computer automatically records all the recordings instead of an independent observer (Lu et al., 2019). The experiment is performed in a dark environment. Rats are placed in cages for 10-minute periods and the system automatically records with infrared rays. After each rat, the cage is cleaned with alcohol to remove odor and urine (Ferah Okkay et al., 2022). **The Elevated Plus Maze Test** is used to measure anxiety-like behaviour in rodents.

The elevated plus maze apparatus is a system consisting of two open arms (without walls; 50 cm × 10 cm) and two closed arms (with black walls, 50 cm × 10 cm). The open and closed arms are connected by a central platform. The labyrinth is 55 cm above the ground. At the start of each test, rats are placed in the central zone and allowed to explore the platform for 5 minutes. The rats are recorded with a camera located at the top of the maze and the test is done in a quiet, dim room. The number of times the rats entered the open and closed arms and the time spent in these arms were recorded. The device was cleaned with an alcohol solution between tests (Chellian et al., 2020; Walf and Frye, 2007). Results are given as arm entries and time spent (durations) in these areas. The more entries into open arms and the more duration spent there, the less anxiety the rat has. The **Passive Avoidance Test** is a system consisting of 2 rooms (light/dark), the base of which is covered with rods that can apply electroshock, in which memory, behaviour and learning abilities are investigated. This system is used to test the learning ability of the animal by fear-driven conditional avoidance. In this test, the animal is expected to learn to avoid entering the electroshock chamber (dark room). Rats are nocturnal animals. By nature, they sleep during the day and are active at night. Although rats are not afraid of light, they generally live in dark compartments because they are uncomfortable with the bright environment. In the passive avoidance system, lighting the bright compartment with LED lights and high lumen light creates an uncomfortable environment for the animals, and they want to move to the closed compartment. Here, the low-intensity electroshock they are exposed to causes a deterrent stimulus and allows the rats to understand and learn how the system works. The experimental procedure is built on these understanding and learning abilities (Gimenez De Bejar et al., 2017; Hosseini et al., 2013; Wu et al., 2020). The experiment is carried out on two consecutive days. Learning is measured on the first day and recall on the second day. The time that each rat took to enter the dark compartment was considered as initial latency. The next day (retention phase), the

rats were reintroduced into the bright chamber and the step-through latency was noted down as memory retention. Shorter latencies indicated poorer cognition. At this stage, rats are expected to remember the shock in the dark compartment. For this reason, it was accepted that the memory of the rats that stayed longer in the bright compartment was stronger. In retention measurements, it is understood that the longer the rats stay in the bright compartment, the stronger the memory and learning.

2.2 RNA extraction and library preparation for transcriptome sequencing

Total RNA is extracted from the snap-frozen rat tissues with Zymo Research Quick RNA Miniprep kit (California USA) by following the protocol provided on the manufacturer's website with slight modifications made to improve the quality and quantity of RNA from each tissue. Before the cell lysis, the tissues are subjected to short (1 min or longer for muscle tissues) homogenization with the beads in PowerLyzer 24 by keeping samples on ice to prevent overheating. The homogenized tissues are further enzymatically in a digestion buffer for at least 30 minutes or more for muscle tissue at room temperature with continuous inversion and agitation of the tubes. After the lysis of the cells, the RNA is cleaned and collected with columns. The quality and quantity of the isolated samples were examined spectrophotometrically with NanoDrop (Thermofisher, USA). After the evaluation of the sample A260, A260/A280, and A260/A230 values, the RNA integrity number (RIN) value of total RNA samples was measured with TapeStation (Agilent Tech, USA). The amount of total RNA was measured more precisely fluorometrically with the RNA Broad Range kit (Thermofisher, USA) by using Qubit (Invitrogen, USA). RNA sequencing library was prepared with Illumina Stranded Total RNA Prep and Ligation with Ribo-Zero Plus kit was used by following the standard protocol provided by the manufacturer. The libraries were then pair-end (2×100bp) sequenced on the NovaSeq6000 system yielding, on average, 25 million fragment reads per sample. Raw sequencing data (.bcl) was converted to FASTQ with

the Dragen Bio-IT platform (v3.9.5). The quality of RNA-seq data was assessed by FastQC (v0.11.9).

2.3 RNA-seq data processing, differential expression, and functional enrichment analysis

Tissue bulk RNA-seq data were aligned and quantified using a standard protocol of Kallisto (v0.46.2) (Bray et al., 2016) against the *Rattus norvegicus* genome (mRatBN7.2) downloaded from Ensembl (Martin et al., 2023) official website (https://www.ensembl.org/index.html). The output of Kallisto, both estimated counts and TPM (transcript per kilobase million)-based transcript-level expressions were then transformed into gene-level expressions using the Bioconductor package tximport (v1.22.0) with the tx2gene option set to connect transcripts to genes (Soneson et al., 2015). Protein-coding genes were considered for the above step and downstream analyses. Differential analysis was performed using the DESeq2 Bioconductor package (v1.34.0) (Love et al., 2014), following a standard protocol for all three pairwise intervention comparisons for determining the effect of sucrose consumption only (sucrose *vs* control), the effect of 30 mg/kg/day JNK-IN-5A treatment (sucrose+JNK_D1 *vs* sucrose), and effect of 60 mg/kg/day JNK-IN-5A treatment (sucrose+JNK_D2 *vs* sucrose) in all four studied tissues. Significantly expressed genes (DEGs) were identified with a significance threshold of an adjusted p-value < 0.01. To examine differences in global gene expression, we conducted principal component analysis (PCA) based on variance-stabilizing transformation (VST)-normalized count data in DESeq2. PC1 and PC2 were plotted for visualization.

Gene Co-expression Network Analysis. For the generation of the tissue-specific co-expression networks, we first filtered out lowly-expressed genes based on their TPM-based expression level (TPM <1) and constructed co-expression networks by generating gene pairs Spearman correlation ranks within the tissue, which was performed using the “spearmanr” function

from *SciPy* (Virtanen et al., 2020) in Python 3.8. Next, considering the network with negative correlation has relatively low correlation scores, we retained the top 10% positively correlated genes that fulfilled FDR < 0.05 on the network (Arif et al., 2021; Yang et al., 2021) and performed module detection analysis using Leiden algorithm (Traag et al., 2019), implemented in the *leidenalg* (v0.7.0) package with “ModularityVertexPartition" to find the optimal partition. Modules with less than 30 genes were discarded to be able to get significant functional analysis results in the downstream analysis. To identify gene modules involved in tissue crosstalk, we correlated the module eigengenes of inter-tissue modules, and assessed the significance of these correlations after Benjamini & Hochberg (BH) correction, with BH-adjusted $p < 0.05$ was considered as significance. The module eigengene is defined as the first principal component of the expression matrix of a given module.

Gene Set Functional Enrichment Analysis. we used Bioconductor package enrichR (v3.2) to annotate gene sets (e.g., differentially expressed genes or co-expression genes) against the curated genes sets obtained from the KEGG pathway database (Kanehisa, 2002), or against hallmark gene sets from MSigDB (Liberzon et al., 2015) using R package msigdbr (v.7.5.1). Benjamini-Hochberg (BH)–adjusted P values (p.adj) < 0.05 are considered as statistically significant and are provided in the relevant figures/datasets.

2.4 Compass-based Metabolic Activity Analysis.

We inferred tissue-level metabolic state from RNA-seq profiles using Compass (Wagner et al., 2021). Compass is a flux balance analysis-based algorithm (Orth et al., 2010) that enables modeling the metabolic state of a system (e.g., single-cell or organ) from RNA-seq data based on a reconstructed genome-scale metabolic model of human metabolism (also known as Recon3D) (Brunk et al., 2018). We downloaded Recon3D from BiGG Models (http://bigg.ucsd.edu/models/Recon3D/) and created model metadata files required for the input of downstream analysis, including gene, reaction, and metabolite metadata, using in-

house scripts. We used human orthologs of rat gene expression data (TPM-based) for computation of the Compass scores matrix using default parameters and the human species as detailed in (Wagner et al., 2021). Downstream analysis was done using the compassR R package (v.1.0.0) following the protocol (https://github.com/YosefLab/compassR).

Statistical Analyses

One-way analysis of variance (ANOVA) test was used to evaluate the significance between the control and treatment groups in behaviour tests using SPSS software (version 20). For the statistical analysis of biometric and plasma parameters, data were shown as mean ± standard deviation (SD), unless stated otherwise. The assumption of normality was determined using the Shapiro–Wilk test. Differences between multiple groups were tested by ANOVA or a non-parametric a non-parametric Kruskal-Wallis test if the data were not normally distributed, followed by Dunn's multiple comparisons post-test. All results were considered statistically significant at $p < 0.05$, unless stated otherwise. A hypergeometric test was used for testing the overlapping between two gene sets. The Jaccard index was used to evaluate the similarity and diversity of two gene sets.

Acknowledgements

The authors would like to acknowledge financial support from ScandiEdge Therapeutics and the Knut and Alice Wallenberg Foundation (No. 72110). A.M. and H.Y. acknowledge support from the PoLiMeR Innovative Training Network (Marie Skłodowska-Curie Grant Agreement No. 812616) which has received funding from the European Union's Horizon 2020 research and innovation program. The computations were performed on resources provided by SNIC through the Uppsala Multidisciplinary Center for Advanced Computational Science (UPPMAX) under Project sllstore2017024 and sctatlas.

Author contributions

A.M. conceived and designed the analysis; M.K., C.B., I.B., O.O.T., C.B., N.Y., S.Y., S.I., J.S., A.H., H.T. collected data for the study; H.Y., C.Z., W.K., M.N.SH. performed the data analysis, visualization, and interpretation; H.Y. drat the manuscript; All authors read and approved the final manuscript.

Declaration of interests

The authors declare no conflict of interest.

Figure Legends

Figure 1. **Schematic representation of experimental setup**. Study groups included the healthy control group received tap water, the sucrose group received 10% sucrose water, the sucrose+JNK_D1 group received 10% sucrose and 30 mg/kg/day JNK-IN-5A, and the sucrose+JNK_D2 group received 10% sucrose and 60 mg/kg/day JNK-IN-5A (N = 44, n = 11 per group).

Figure 2. **Sucrose consumption and JNK-IN-5A treatment exhibit distinct effects on the mRNA expression of genes encoding JNK isoforms in the major metabolic tissues. (a)** The acute effect of JNK-IN-5A in rats (n = 3/Sex/Group). Statistically significant changed clinical chemistry parameters were presented as mean ± standard deviation (SD), see also **Data S1**. ALB: albumin; ALP: alkaline phosphatase; BUN: blood urea nitrogen; PHOS: phosphate; GLU: glucose; K^+: potassium; Na^+: sodium; TP: total Protein; GLOB: globulin. Statistical significance was assessed by one-way ANOVA testing followed by Dunn's multiple comparisons post-test, *p*-value < 0.05 is considered as statistical significance. (**b**) Boxplot showing the levels of plasma triglycerides in control, sucrose, sucrose+JNK_D1, and sucrose+JNK_D2 rats. Statistical significance was assessed by one-way ANOVA testing followed by Dunn's multiple comparisons post-test, *p*-value < 0.05 is considered as statistical significance. * $p < 0.05$, ** $p < 0.01$, *** $p < 0.001$, **** $p < 0.0001$. (**c**) Boxplot showing the relative mRNA expression of *Mapk8*, *Mapk9*, and *Mapk10* in the studied tissues. The count-based abundance of genes was transformed using the vst function and the adjusted *p*-value (p.adj) is derived from DESeq2 (Love et al., 2014). * p.adj < 0.05, ** p.adj < 0.01, *** p.adj < 0.001, **** p.adj < 0.0001. (**d**) Correlation between the relative mRNA expression of *Mapk8* and (**e**) *Mapk9* in skeletal muscle tissue (SkM) and plasma triglycerides level.

Figure 3. **System-wide transcriptomics profiling revealed tissue-specific metabolic rewiring by sucrose consumption and JNK-IN-5A treatment** (**a**) Principal component

analysis (PCA) of liver, vWAT, SkM, and brain transcriptome data showing global gene expression profiles in control (n = 9), sucrose (n = 11), sucrose+JNK_D1 and sucrose+JNK_D2 (n = 10/per group). Each data point represents a sample in the respective coloured group. (**b**) Bar graphs represent the percentage of differential expressed genes (or regulated genes) associated with sucrose (sucrose *vs.* control), sucrose+JNK_D1 (sucrose+JNK_D1 *vs.* sucrose), or sucrose+JNK_D2 (sucrose+JNK_D2 *vs.* sucrose) in all protein-coding genes (N = 19,780) for each tissue. (**c**) Heatmap of all genes differentially upregulated (red) and downregulated (blue) in three pairwise comparisons for sucrose (sucrose *vs.* control), sucrose+JNK_D1 (sucrose+JNK_D1 *vs.* sucrose), and sucrose+JNK_D2 (sucrose+JNK_D2 *vs.* sucrose) (adjusted *p*-value, p.adj < 0.01) for each tissue. Column annotation represents tissues. (**d**) Venn diagram showing the overlap between significantly regulated genes response to sucrose consumption and JNK_D1 treatment, see also **Fig. S1**.

Figure 4. JNK inhibition in SkM correlated with the regulation of energy metabolism in the liver and adipose tissues. (**a-b**) Venn diagram showing the overlap between significantly regulated genes response to sucrose consumption and INK_D1 treatment in SkM, see also **Fig. S1&Fig. S5**. (**c-d**) Functional annotation of up- (red) and down-regulated (blue) genes in JNK_D1-treated SkM with a Benjamini Hochberg adjusted p-value < 0.05. (**e**) Correlation of $\log_2$(Fold change) for shared DEGs between the SkM and Liver, vWAT, or Brain after JNK_D1 treatment.

Figure 5. **JNK inhibition regulates insulin signalling-related genes in SkM** (**a**) A representative diagram of metabolic pathways associated with insulin resistance and insulin signalling was found to be largely inhibited by JNK_D1 treatment. (**b**) Correlation between the relative mRNA expression of *Phkg1, Phkb, and Ppp1r3f* (those three genes are also significantly upregulated in sucrose-feeding only group) in SkM and plasma triglycerides

level. (**c**) Relative changes of genes involved in insulin resistance and insulin signalling pathways in response to sucrose consumption and JNK-IN-5A treatment in the tissues. The adjusted *p*-value (p.adj) is derived from DESeq2 (Love et al., 2014). * p.adj < 0.05, ** p.adj < 0.01, *** p.adj < 0.001, **** p.adj < 0.0001.

Figure 6. Inter-tissue network analysis identifies JNK-IN-5A inhibition-associated molecular mechanism. (**a**) Significantly enriched modules (hypergeometric test, p < 0.05) by the differentially expressed genes related to sucrose, sucrose+JNK_D1 and sccrose+JNK_D1 in each tissue. (**b**) Dot-plot showing the significant correlation among inter-tissue module pairs. The size and colour of the connected line are proportional to the correlation coefficient and statistical significance indicated by the adjusted *p*-value. The module pairs with Benjamini Hochberg adjusted p-value (p.adj) < 0.05 are presented. (**c**) Spearman coefficient correlation of the first component from PCA analyses on gene expression of module pairs. (**d**) Significantly enriched MSigDB hallmark gene sets by each module.

Figure 7. **Metabolic modelling highlights metabolic reprogramming linked to JNK-IN-5A inhibition** (**a**) The numbers of differentially altered metabolic reactions in response to sucrose, sucrose+JNK_D1, and sucrose+JNK_D2, respectively, see also **Data S13**. (**b**) Distribution of Cohen's d statistic for differential metabolic reactions in response to sucrose, sucrose+JNK_D1 and sucrose+JNK_D2 in each tissue, see also **Data S13**. (**c**) Principal component analysis of the Compass score of metabolic reaction potential activity scores showing the metabolic heterogeneity in response to sucrose ingestion and JNK-IN-5A treatment at the tissue levels, for principal components 1 and 2. (**d**) Heatmap showing the tissue-level differential activity of metabolic reactions in response to sucrose intake and JNK-IN-5A treatment. Reactions are partitioned by Recon3 pathways (Brunk et al., 2018) and coloured by the sign of their Cohen's d statistic derived from different contrasts: sucrose *vs*

control, sucrose+JNK_D1 *vs* sucrose, or sucrose+JNK_D2 vs sucrose, respectively. Abbreviations: vWAT, visceral white adipose tissue; SkM, skeletal muscle.

Supplementary Figure Legends

Figure S1. (**a**) Gene expression pattern of JNK isoforms (**b-e**) UpSet plot showing the number of shared differentially expressed genes (DEGs) (adjusted-p < 0.01) associated with sucrose consumption and JNK-IN-5A treatment in the liver, visceral white adipose tissue (vWAT), skeletal muscle tissue (SkM) and brain tissues in the experimental rats. The histogram bar graph (right) shows the total number of DEGs in each comparison corresponding. The histogram bar graph (top) shows the number of DEGs shared among pairwise comparisons. Connected lines indicate what comparisons are sharing DEGs.

Figure S2. (**a**) Venn diagram showing the overlap between significantly regulated genes response to sucrose consumption and JNK_D2 treatment in liver and (**b**) in vWAT, related to **Fig. 3**. (**c**) Top-10 enriched KEGG pathways enriched by reversed genes after JNK_D1 treatment in liver and (**d**) in vWAT.

Figure S3. Relative changes of genes involved in fatty acid degradation, elongation, biosynthesis, and metabolism in response to sucrose consumption and JNK-IN-5A treatment in the tissues, related to **Fig. 2**.

Figure S4. Relative changes of genes involved in fatty acid uptake in response to sucrose consumption and JNK-in-5A treatment in the tissues, related to **Fig. 2**.

Figure S5. Relative changes of genes involved in redox homeostasis in response to sucrose consumption and JNK-in-5A treatment in the tissues, related to **Fig. 2**.

Figure S6. (**a**) Venn diagram showing the overlap between significantly regulated genes response to sucrose consumption and JNK_D2 treatment in SkM, see also **Fig. S1&Fig. S5**. (**b**) Correlation of $\log_2$(Fold change) for shared DEGs between the SkM and Liver, vWAT, or Brain after JNK_D2 treatment. (c) Venn diagram showing the overlap between significantly

regulated genes response to sucrose consumption and JNK_D1 treatment as well as (**d**) JNK_D2 treatment in the Brain, respectively.

Figure S7. (**a**) The number of gene modules are identified from the tissue-specific co-expression networks. The text on the module indicates the module name and the number of genes of individual modules in each tissue. The edges between the clusters were aggregations of the inter-cluster edges. (**b**) PCA of Liver.M0, vWAT.M3, and SkM.M0 gene expression data. (**c**) Module neighbors of Mapk9 in SkM.M0.

Supplementary Dataset and Tables

Data S1: Summary of body weight and clinical pathological parameters for 7 days oral toxicology of JNK-IN-5A in rats.

Data S2: Summary of body weight and clinical pathological parameters for 3 weeks oral administration of JNK-IN-5A in MAFLD rats model.

Data S3: Passive avoidance data.

Data S4: Locomotor activity data.

Data S5: Elevated plus maze data.

Data S6: Result of differential expression analysis for all relevant comparisons of liver, white adipose tissue, skeletal muscle and brain in the study, related to **Fig. 2-4**.

Data S7: Gene membership in certain module identified from the tissue-specific co-expression networks, which includes samples from Control, Sucrose and Sucrose+JNK_D1 groups, related to **Fig. 6**.

Data S8: Results of genome-scale metabolic modelling based on Compass and Recon3D, related to **Fig. 7**.

Reference

Angell, R. M., Atkinson, F. L., Brown, M. J., Chuang, T. T., Christopher, J. A., Cichy-Knight, M., Dunn, A. K., Hightower, K. E., Malkakorpi, S., Musgrave, J. R., Neu, M., Rowland, P., Shea, R. L., Smith, J. L., Somers, D. O., Thomas, S. A., Thompson, G., Wang, R., 2007. N-(3-Cyano-4,5,6,7-tetrahydro-1-benzothien-2-yl)amides as potent, selective, inhibitors of JNK2 and JNK3. Bioorg Med Chem Lett. 17**,** 1296-301.

Arif, M., Klevstig, M., Benfeitas, R., Doran, S., Turkez, H., Uhlen, M., Clausen, M., Wikstrom, J., Etal, D., Zhang, C., Levin, M., Mardinoglu, A., Boren, J., 2021. Integrative transcriptomic analysis of tissue-specific metabolic crosstalk after myocardial infarction. Elife. 10.

Azzu, V., Vacca, M., Virtue, S., Allison, M., Vidal-Puig, A., 2020. Adipose Tissue-Liver Cross Talk in the Control of Whole-Body Metabolism: Implications in Nonalcoholic Fatty Liver Disease. Gastroenterology. 158**,** 1899-1912.

Barabasi, A. L., Albert, R., 1999. Emergence of scaling in random networks. Science. 286**,** 509-12.

Bray, N. L., Pimentel, H., Melsted, P., Pachter, L., 2016. Near-optimal probabilistic RNA-seq quantification. Nat Biotechnol. 34**,** 525-7.

Brunk, E., Sahoo, S., Zielinski, D. C., Altunkaya, A., Drager, A., Mih, N., Gatto, F., Nilsson, A., Preciat Gonzalez, G. A., Aurich, M. K., Prlic, A., Sastry, A., Danielsdottir, A. D., Heinken, A., Noronha, A., Rose, P. W., Burley, S. K., Fleming, R. M. T., Nielsen, J., Thiele, I., Palsson, B. O., 2018. Recon3D enables a three-dimensional view of gene variation in human metabolism. Nat Biotechnol. 36**,** 272-281.

Califano, A., Butte, A. J., Friend, S., Ideker, T., Schadt, E., 2012. Leveraging models of cell regulation and GWAS data in integrative network-based association studies. Nat Genet. 44**,** 841-7.

Cerbone, A., Toaldo, C., Pizzimenti, S., Pettazzoni, P., Dianzani, C., Minelli, R., Ciamporcero, E., Roma, G., Dianzani, M. U., Canaparo, R., Ferretti, C., Barrera, G., 2012. AS601245, an Anti-Inflammatory JNK Inhibitor, and Clofibrate Have a Synergistic Effect in Inducing Cell Responses and in Affecting the Gene Expression Profile in CaCo-2 Colon Cancer Cells. PPAR Res. 2012**,** 269751.

Chang, L., Karin, M., 2001. Mammalian MAP kinase signalling cascades. Nature. 410**,** 37-40.

Chellian, R., Behnood-Rod, A., Wilson, R., Wilks, I., Knight, P., Febo, M., Bruijnzeel, A. W., 2020. Exposure to smoke from high- but not low-nicotine cigarettes leads to signs of dependence in male rats and potentiates the effects of nicotine in female rats. Pharmacol Biochem Behav. 196**,** 172998.

Choobdar, S., Ahsen, M. E., Crawford, J., Tomasoni, M., Fang, T., Lamparter, D., Lin, J., Hescott, B., Hu, X., Mercer, J., Natoli, T., Narayan, R., Consortium, D. M. I. C., Subramanian, A., Zhang, J. D., Stolovitzky, G., Kutalik, Z., Lage, K., Slonim, D. K., Saez-Rodriguez, J., Cowen, L. J., Bergmann, S., Marbach, D., 2019. Assessment of network module identification across complex diseases. Nat Methods. 16**,** 843-852.

Czaja, M. J., 2010. JNK regulation of hepatic manifestations of the metabolic syndrome. Trends Endocrinol Metab. 21**,** 707-13.

Dobrin, R., Zhu, J., Molony, C., Argman, C., Parrish, M. L., Carlson, S., Allan, M. F., Pomp, D., Schadt, E. E., 2009. Multi-tissue coexpression networks reveal unexpected subnetworks associated with disease. Genome Biol. 10**,** R55.

731 Ferah Okkay, I., Okkay, U., Gundogdu, O. L., Bayram, C., Mendil, A. S., Ertugrul, M. S.,
732 Hacimuftuoglu, A., 2022. Syringic acid protects against thioacetamide-induced
733 hepatic encephalopathy: Behavioral, biochemical, and molecular evidence. Neurosci
734 Lett. 769, 136385.
735 Geidl-Flueck, B., Hochuli, M., Nemeth, A., Eberl, A., Derron, N., Kofeler, H. C., Tappy, L.,
736 Berneis, K., Spinas, G. A., Gerber, P. A., 2021. Fructose- and sucrose- but not glucose-
737 sweetened beverages promote hepatic de novo lipogenesis: A randomized
738 controlled trial. J Hepatol. 75, 46-54.
739 Geurtsen, M. L., Santos, S., Gaillard, R., Felix, J. F., Jaddoe, V. W. V., 2021. Associations
740 Between Intake of Sugar-Containing Beverages in Infancy With Liver Fat
741 Accumulation at School Age. Hepatology. 73, 560-570.
742 Gimenez De Bejar, V., Caballero Bleda, M., Popovic, N., Popovic, M., 2017. Verapamil Blocks
743 Scopolamine Enhancement Effect on Memory Consolidation in Passive Avoidance
744 Task in Rats. Front Pharmacol. 8, 566.
745 Hosseini, N., Alaei, H., Reisi, P., Radahmadi, M., 2013. The effect of treadmill running on
746 passive avoidance learning in animal model of Alzheimer disease. Int J Prev Med. 4,
747 187-92.
748 Jang, C., Wada, S., Yang, S., Gosis, B., Zeng, X., Zhang, Z., Shen, Y., Lee, G., Arany, Z.,
749 Rabinowitz, J. D., 2020. The small intestine shields the liver from fructose-induced
750 steatosis. Nat Metab. 2, 586-593.
751 Jeon, Y. G., Kim, Y. Y., Lee, G., Kim, J. B., 2023. Physiological and pathological roles of
752 lipogenesis. Nat Metab. 5, 735-759.
753 Kanehisa, M., 2002. The KEGG database. Novartis Found Symp. 247, 91-101; discussion 101-
754 3, 119-28, 244-52.
755 Karlsen, T. H., Sheron, N., Zelber-Sagi, S., Carrieri, P., Dusheiko, G., Bugianesi, E., Pryke, R.,
756 Hutchinson, S. J., Sangro, B., Martin, N. K., Cecchini, M., Dirac, M. A., Belloni, A.,
757 Serra-Burriel, M., Ponsioen, C. Y., Sheena, B., Lerouge, A., Devaux, M., Scott, N.,
758 Hellard, M., Verkade, H. J., Sturm, E., Marchesini, G., Yki-Jarvinen, H., Byrne, C. D.,
759 Targher, G., Tur-Sinai, A., Barrett, D., Ninburg, M., Reic, T., Taylor, A., Rhodes, T.,
760 Treloar, C., Petersen, C., Schramm, C., Flisiak, R., Simonova, M. Y., Pares, A., Johnson,
761 P., Cucchetti, A., Graupera, I., Lionis, C., Pose, E., Fabrellas, N., Ma, A. T., Mendive, J.
762 M., Mazzaferro, V., Rutter, H., Cortez-Pinto, H., Kelly, D., Burton, R., Lazarus, J. V.,
763 Gines, P., Buti, M., Newsome, P. N., Burra, P., Manns, M. P., 2022. The EASL-Lancet
764 Liver Commission: protecting the next generation of Europeans against liver disease
765 complications and premature mortality. Lancet. 399, 61-116.
766 Kim, W., Li, M., Jin, H., Yang, H., Turkez, H., Uhlen, M., Zhang, C., Mardinoglu, A., 2023.
767 Characterization of an in vitro steatosis model simulating activated de novo
768 lipogenesis in MAFLD patients. iScience. 26, 107727.
769 Kodama, Y., Brenner, D. A., 2009. c-Jun N-terminal kinase signaling in the pathogenesis of
770 nonalcoholic fatty liver disease: Multiple roles in multiple steps. Hepatology. 49, 6-8.
771 Kotsiliti, E., 2023. NAFLD incidence is increasing. Nat Rev Gastroenterol Hepatol. 20, 344.
772 Le, M. H., Le, D. M., Baez, T. C., Wu, Y., Ito, T., Lee, E. Y., Lee, K., Stave, C. D., Henry, L.,
773 Barnett, S. D., Cheung, R., Nguyen, M. H., 2023. Global incidence of non-alcoholic
774 fatty liver disease: A systematic review and meta-analysis of 63 studies and
775 1,201,807 persons. J Hepatol. 79, 287-295.

776 Lessard, S. J., MacDonald, T. L., Pathak, P., Han, M. S., Coffey, V. G., Edge, J., Rivas, D. A.,
777 Hirshman, M. F., Davis, R. J., Goodyear, L. J., 2018. JNK regulates muscle remodeling
778 via myostatin/SMAD inhibition. Nat Commun. 9**,** 3030.
779 Liberzon, A., Birger, C., Thorvaldsdottir, H., Ghandi, M., Mesirov, J. P., Tamayo, P., 2015. The
780 Molecular Signatures Database (MSigDB) hallmark gene set collection. Cell Syst. 1**,**
781 417-425.
782 Llovet, J. M., Willoughby, C. E., Singal, A. G., Greten, T. F., Heikenwalder, M., El-Serag, H. B.,
783 Finn, R. S., Friedman, S. L., 2023. Nonalcoholic steatohepatitis-related hepatocellular
784 carcinoma: pathogenesis and treatment. Nat Rev Gastroenterol Hepatol.
785 Love, M. I., Huber, W., Anders, S., 2014. Moderated estimation of fold change and
786 dispersion for RNA-seq data with DESeq2. Genome Biol. 15**,** 550.
787 Lu, Y., Sareddy, G. R., Wang, J., Wang, R., Li, Y., Dong, Y., Zhang, Q., Liu, J., O'Connor, J. C., Xu,
788 J., Vadlamudi, R. K., Brann, D. W., 2019. Neuron-Derived Estrogen Regulates Synaptic
789 Plasticity and Memory. J Neurosci. 39**,** 2792-2809.
790 Machado, M. V., Cortez-Pinto, H., 2023. NAFLD, MAFLD and obesity: brothers in arms? Nat
791 Rev Gastroenterol Hepatol. 20**,** 67-68.
792 Malik, V. S., Hu, F. B., 2022. The role of sugar-sweetened beverages in the global epidemics
793 of obesity and chronic diseases. Nat Rev Endocrinol. 18**,** 205-218.
794 Mardinoglu, A., Agren, R., Kampf, C., Asplund, A., Nookaew, I., Jacobson, P., Walley, A. J.,
795 Froguel, P., Carlsson, L. M., Uhlen, M., Nielsen, J., 2013. Integration of clinical data
796 with a genome-scale metabolic model of the human adipocyte. Mol Syst Biol. 9**,** 649.
797 Mardinoglu, A., Boren, J., Smith, U., Uhlen, M., Nielsen, J., 2018. Systems biology in
798 hepatology: approaches and applications. Nat Rev Gastroenterol Hepatol. 15**,** 365-
799 377.
800 Mardinoglu, A., Nielsen, J., 2012. Systems medicine and metabolic modelling. J Intern Med.
801 271**,** 142-54.
802 Martin, F. J., Amode, M. R., Aneja, A., Austine-Orimoloye, O., Azov, A. G., Barnes, I., Becker,
803 A., Bennett, R., Berry, A., Bhai, J., Bhurji, S. K., Bignell, A., Boddu, S., Branco Lins, P. R.,
804 Brooks, L., Ramaraju, S. B., Charkhchi, M., Cockburn, A., Da Rin Fiorretto, L., Davidson,
805 C., Dodiya, K., Donaldson, S., El Houdaigui, B., El Naboulsi, T., Fatima, R., Giron, C. G.,
806 Genez, T., Ghattaoraya, G. S., Martinez, J. G., Guijarro, C., Hardy, M., Hollis, Z.,
807 Hourlier, T., Hunt, T., Kay, M., Kaykala, V., Le, T., Lemos, D., Marques-Coelho, D.,
808 Marugan, J. C., Merino, G. A., Mirabueno, L. P., Mushtaq, A., Hossain, S. N., Ogeh, D.
809 N., Sakthivel, M. P., Parker, A., Perry, M., Pilizota, I., Prosovetskaia, I., Perez-Silva, J.
810 G., Salam, A. I. A., Saraiva-Agostinho, N., Schuilenburg, H., Sheppard, D., Sinha, S.,
811 Sipos, B., Stark, W., Steed, E., Sukumaran, R., Sumathipala, D., Suner, M. M.,
812 Surapaneni, L., Sutinen, K., Szpak, M., Tricomi, F. F., Urbina-Gomez, D., Veidenberg,
813 A., Walsh, T. A., Walts, B., Wass, E., Willhoft, N., Allen, J., Alvarez-Jarreta, J.,
814 Chakiachvili, M., Flint, B., Giorgetti, S., Haggerty, L., Ilsley, G. R., Loveland, J. E.,
815 Moore, B., Mudge, J. M., Tate, J., Thybert, D., Trevanion, S. J., Winterbottom, A.,
816 Frankish, A., Hunt, S. E., Ruffier, M., Cunningham, F., Dyer, S., Finn, R. D., Howe, K. L.,
817 Harrison, P. W., Yates, A. D., Flicek, P., 2023. Ensembl 2023. Nucleic Acids Res. 51**,**
818 D933-D941.
819 Nassir, F., Rector, R. S., Hammoud, G. M., Ibdah, J. A., 2015. Pathogenesis and Prevention of
820 Hepatic Steatosis. Gastroenterol Hepatol (N Y). 11**,** 167-75.
821 Nikolic, I., Leiva, M., Sabio, G., 2020. The role of stress kinases in metabolic disease. Nat Rev
822 Endocrinol. 16**,** 697-716.

823 Orth, J. D., Thiele, I., Palsson, B. O., 2010. What is flux balance analysis? Nat Biotechnol. 28,
824 245-8.
825 Sabio, G., Cavanagh-Kyros, J., Ko, H. J., Jung, D. Y., Gray, S., Jun, J. Y., Barrett, T., Mora, A.,
826 Kim, J. K., Davis, R. J., 2009. Prevention of steatosis by hepatic JNK1. Cell Metab. 10,
827 491-8.
828 Sabio, G., Davis, R. J., 2010. cJun NH2-terminal kinase 1 (JNK1): roles in metabolic regulation
829 of insulin resistance. Trends Biochem Sci. 35, 490-6.
830 Schattenberg, J. M., Singh, R., Wang, Y., Lefkowitch, J. H., Rigoli, R. M., Scherer, P. E., Czaja,
831 M. J., 2006. JNK1 but not JNK2 promotes the development of steatohepatitis in mice.
832 Hepatology. 43, 163-72.
833 Seki, E., Brenner, D. A., Karin, M., 2012. A liver full of JNK: signaling in regulation of cell
834 function and disease pathogenesis, and clinical approaches. Gastroenterology. 143,
835 307-20.
836 Singh, R., Wang, Y., Xiang, Y., Tanaka, K. E., Gaarde, W. A., Czaja, M. J., 2009. Differential
837 effects of JNK1 and JNK2 inhibition on murine steatohepatitis and insulin resistance.
838 Hepatology. 49, 87-96.
839 Softic, S., Stanhope, K. L., Boucher, J., Divanovic, S., Lanaspa, M. A., Johnson, R. J., Kahn, C. R.,
840 2020. Fructose and hepatic insulin resistance. Crit Rev Clin Lab Sci. 57, 308-322.
841 Solinas, G., Becattini, B., 2017. JNK at the crossroad of obesity, insulin resistance, and cell
842 stress response. Mol Metab. 6, 174-184.
843 Soneson, C., Love, M. I., Robinson, M. D., 2015. Differential analyses for RNA-seq: transcript-
844 level estimates improve gene-level inferences. F1000Res. 4, 1521.
845 Sousa, R. M. L., Ribeiro, N. L. X., Pinto, B. A. S., Sanches, J. R., da Silva, M. U., Coelho, C. F. F.,
846 Franca, L. M., de Figueiredo Neto, J. A., Paes, A. M. A., 2018. Long-term high-protein
847 diet intake reverts weight gain and attenuates metabolic dysfunction on high-
848 sucrose-fed adult rats. Nutr Metab (Lond). 15, 53.
849 Stephenson, E. J., Stayton, A. S., Sethuraman, A., Rao, P. K., Meyer, A., Gomes, C. K.,
850 Mulcahy, M. C., McAllan, L., Puchowicz, M. A., Pierre, J. F., Bridges, D., Han, J. C.,
851 2022. Chronic intake of high dietary sucrose induces sexually dimorphic metabolic
852 adaptations in mouse liver and adipose tissue. Nat Commun. 13, 6062.
853 Sveinbjornsson, G., Ulfarsson, M. O., Thorolfsdottir, R. B., Jonsson, B. A., Einarsson, E.,
854 Gunnlaugsson, G., Rognvaldsson, S., Arnar, D. O., Baldvinsson, M., Bjarnason, R. G.,
855 consortium, D. G., Eiriksdottir, T., Erikstrup, C., Ferkingstad, E., Halldorsson, G. H.,
856 Helgason, H., Helgadottir, A., Hindhede, L., Hjorleifsson, G., Jones, D., Knowlton, K. U.,
857 Lund, S. H., Melsted, P., Norland, K., Olafsson, I., Olafsson, S., Oskarsson, G. R.,
858 Ostrowski, S. R., Pedersen, O. B., Snaebjarnarson, A. S., Sigurdsson, E.,
859 Steinthorsdottir, V., Schwinn, M., Thorgeirsson, G., Thorleifsson, G., Jonsdottir, I.,
860 Bundgaard, H., Nadauld, L., Bjornsson, E. S., Rulifson, I. C., Rafnar, T., Norddahl, G. L.,
861 Thorsteinsdottir, U., Sulem, P., Gudbjartsson, D. F., Holm, H., Stefansson, K., 2022.
862 Multiomics study of nonalcoholic fatty liver disease. Nat Genet. 54, 1652-1663.
863 Traag, V. A., Waltman, L., van Eck, N. J., 2019. From Louvain to Leiden: guaranteeing well-
864 connected communities. Sci Rep. 9, 5233.
865 Vernia, S., Cavanagh-Kyros, J., Garcia-Haro, L., Sabio, G., Barrett, T., Jung, D. Y., Kim, J. K., Xu,
866 J., Shulha, H. P., Garber, M., Gao, G., Davis, R. J., 2014. The PPARalpha-FGF21
867 hormone axis contributes to metabolic regulation by the hepatic JNK signaling
868 pathway. Cell Metab. 20, 512-25.

Virtanen, P., Gommers, R., Oliphant, T. E., Haberland, M., Reddy, T., Cournapeau, D., Burovski, E., Peterson, P., Weckesser, W., Bright, J., van der Walt, S. J., Brett, M., Wilson, J., Millman, K. J., Mayorov, N., Nelson, A. R. J., Jones, E., Kern, R., Larson, E., Carey, C. J., Polat, I., Feng, Y., Moore, E. W., VanderPlas, J., Laxalde, D., Perktold, J., Cimrman, R., Henriksen, I., Quintero, E. A., Harris, C. R., Archibald, A. M., Ribeiro, A. H., Pedregosa, F., van Mulbregt, P., SciPy, C., 2020. SciPy 1.0: fundamental algorithms for scientific computing in Python. Nat Methods. 17**,** 261-272.

Wagner, A., Wang, C., Fessler, J., DeTomaso, D., Avila-Pacheco, J., Kaminski, J., Zaghouani, S., Christian, E., Thakore, P., Schellhaass, B., Akama-Garren, E., Pierce, K., Singh, V., Ron-Harel, N., Douglas, V. P., Bod, L., Schnell, A., Puleston, D., Sobel, R. A., Haigis, M., Pearce, E. L., Soleimani, M., Clish, C., Regev, A., Kuchroo, V. K., Yosef, N., 2021. Metabolic modeling of single Th17 cells reveals regulators of autoimmunity. Cell. 184**,** 4168-4185 e21.

Walf, A. A., Frye, C. A., 2007. The use of the elevated plus maze as an assay of anxiety-related behavior in rodents. Nat Protoc. 2**,** 322-8.

Wu, C., Yang, L., Li, Y., Dong, Y., Yang, B., Tucker, L. D., Zong, X., Zhang, Q., 2020. Effects of Exercise Training on Anxious-Depressive-like Behavior in Alzheimer Rat. Med Sci Sports Exerc. 52**,** 1456-1469.

Xiao, X., Lai, W., Xie, H., Liu, Y., Guo, W., Liu, Y., Li, Y., Li, Y., Zhang, J., Chen, W., Shi, M., Shang, L., Yin, M., Wang, C., Deng, H., 2019. Targeting JNK pathway promotes human hematopoietic stem cell expansion. Cell Discov. 5**,** 2.

Yang, H., Arif, M., Yuan, M., Li, X., Shong, K., Turkez, H., Nielsen, J., Uhlen, M., Boren, J., Zhang, C., Mardinoglu, A., 2021. A network-based approach reveals the dysregulated transcriptional regulation in non-alcoholic fatty liver disease. iScience. 24**,** 103222.

Yang, Y., Han, L., Yuan, Y., Li, J., Hei, N., Liang, H., 2014. Gene co-expression network analysis reveals common system-level properties of prognostic genes across cancer types. Nat Commun. 5**,** 3231.

Yki-Jarvinen, H., Luukkonen, P. K., Hodson, L., Moore, J. B., 2021. Dietary carbohydrates and fats in nonalcoholic fatty liver disease. Nat Rev Gastroenterol Hepatol. 18**,** 770-786.

Younossi, Z. M., Golabi, P., Paik, J. M., Henry, A., Van Dongen, C., Henry, L., 2023. The global epidemiology of nonalcoholic fatty liver disease (NAFLD) and nonalcoholic steatohepatitis (NASH): a systematic review. Hepatology. 77**,** 1335-1347.

Zhang, C., Lee, S., Mardinoglu, A., Hua, Q., 2016. Investigating the Combinatory Effects of Biological Networks on Gene Co-expression. Front Physiol. 7**,** 160.

Zhang, S., Gu, Y., Bian, S., Lu, Z., Zhang, Q., Liu, L., Meng, G., Yao, Z., Wu, H., Wang, Y., Zhang, T., Wang, X., Sun, S., Wang, X., Zhou, M., Jia, Q., Song, K., Qi, L., Niu, K., 2021. Soft drink consumption and risk of nonalcoholic fatty liver disease: results from the Tianjin Chronic Low-Grade Systemic Inflammation and Health (TCLSIH) cohort study. Am J Clin Nutr. 113**,** 1265-1274.

Figure 1. Study overview

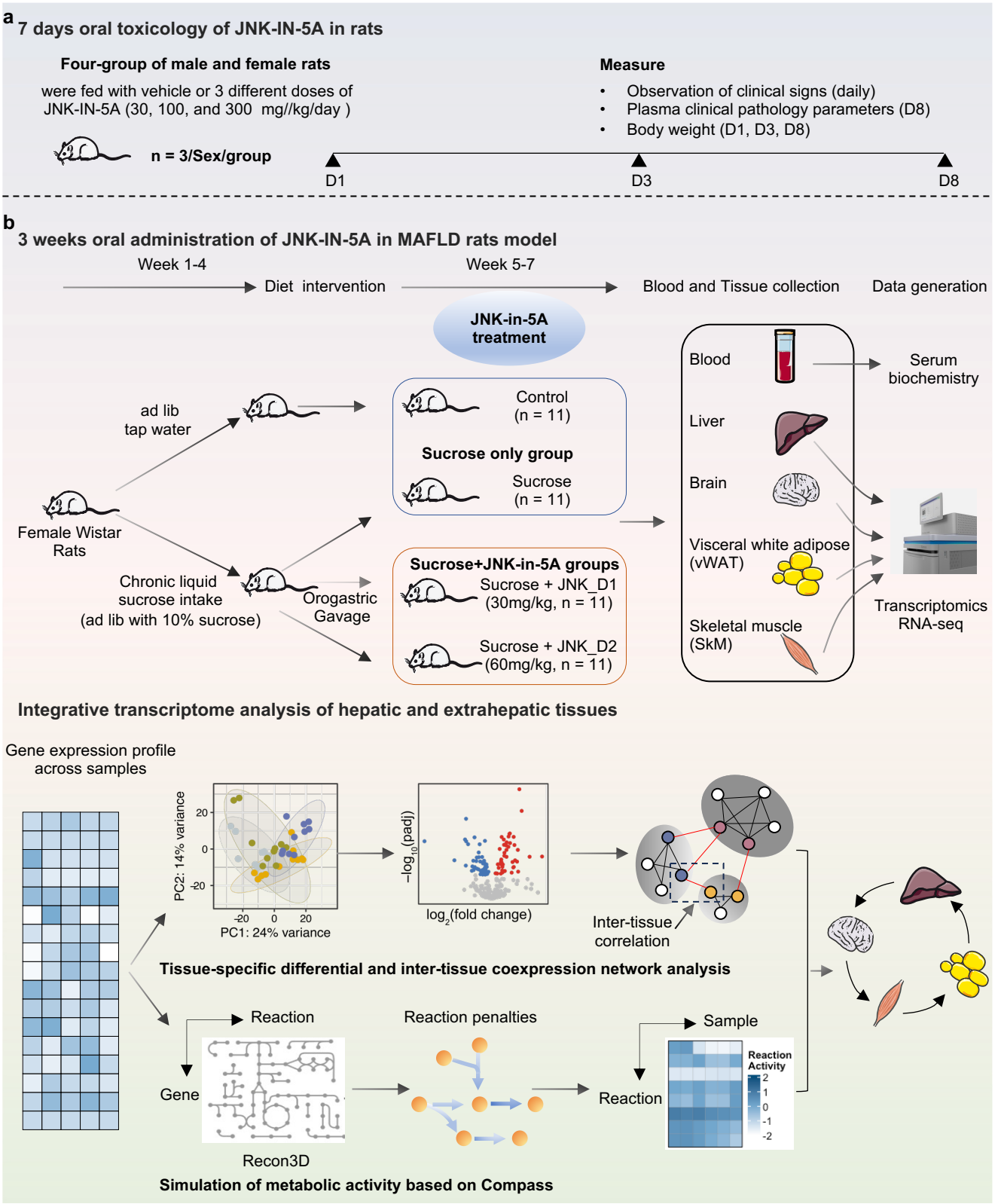

Figure 2. JNK-in-5A treatment exhibit distinct effects on the mRNA expression of genes encoding JNK isoforms

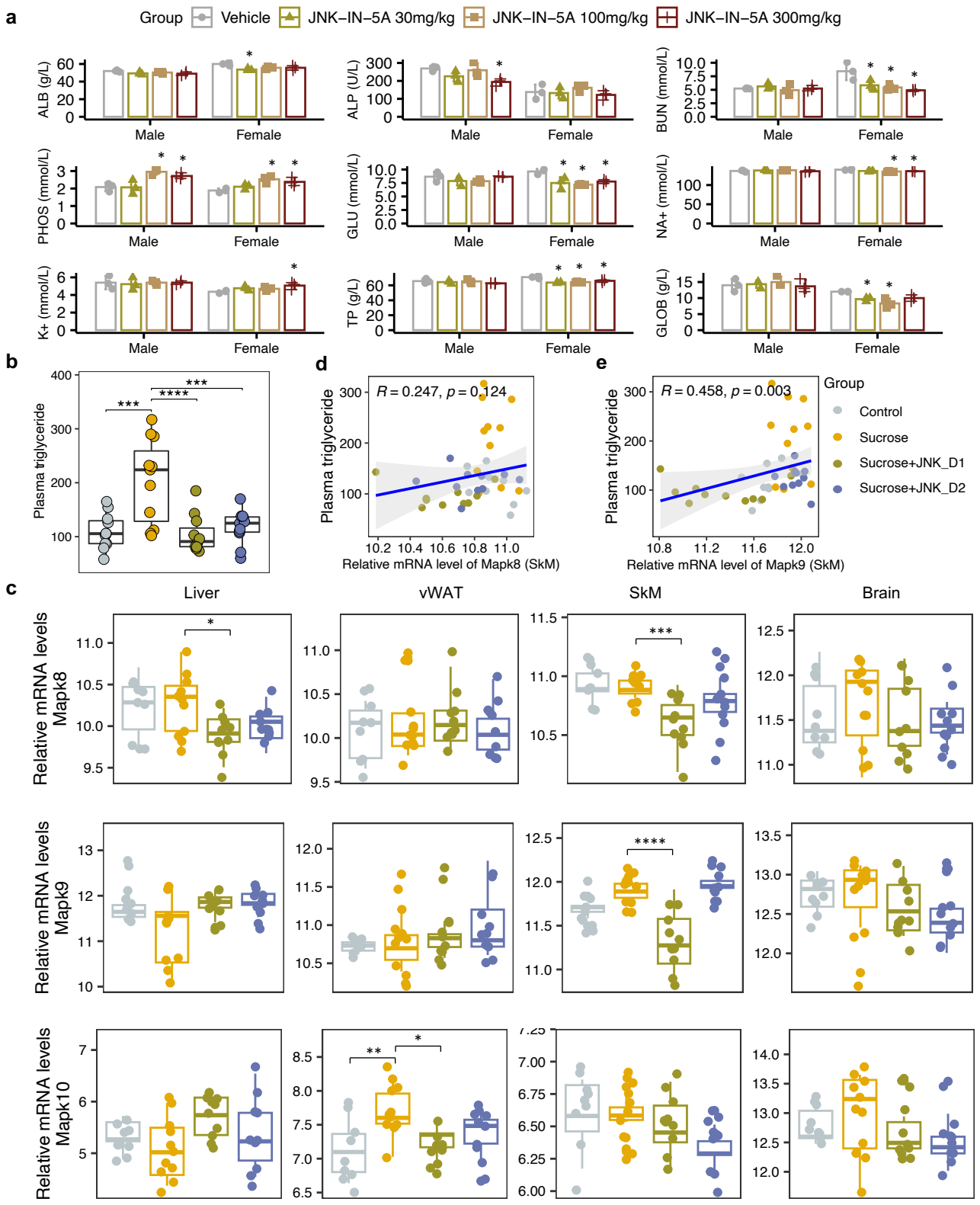

Figure 3. System-wide transcriptomics profiling revealed tissue-specific metabolic rewiring by sucrose consumption and JNK-in-5A treatment

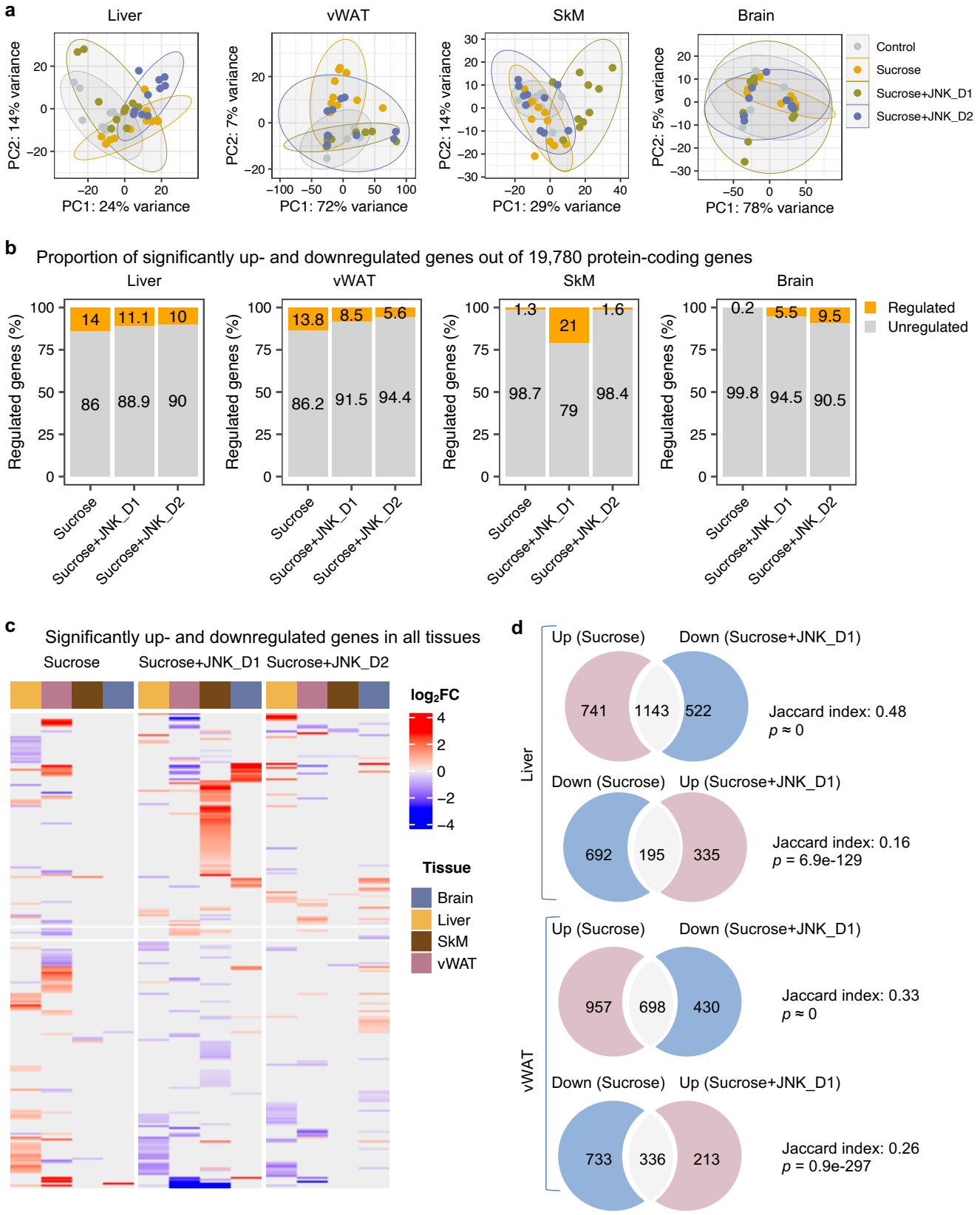

Figure 4. JNK inhibition in SkM correlated with the regulation of energy metabolism in liver and adipose tissues

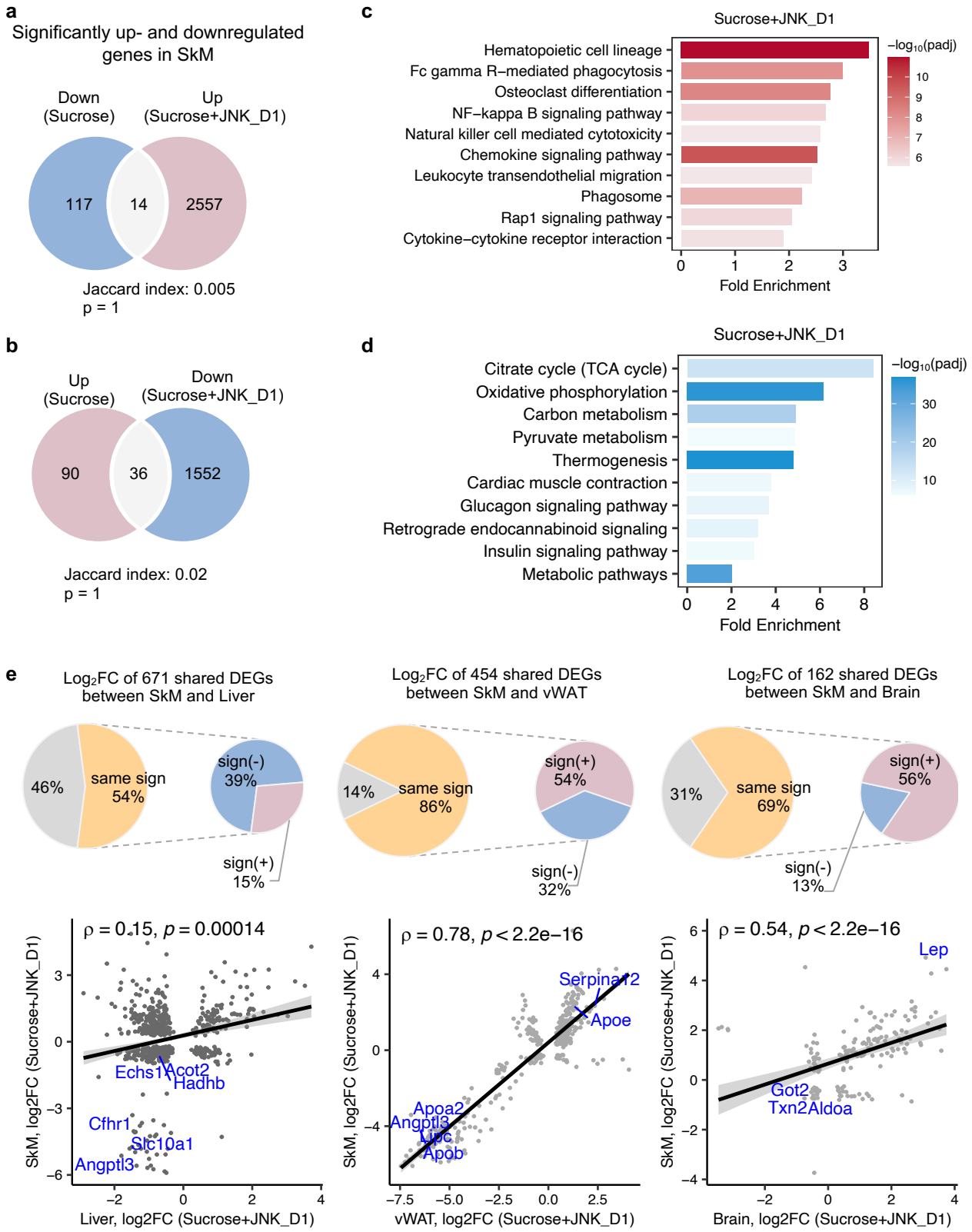

Figure 5. JNK inhibition regulates insulin signalling-related genes in skeletal muscle

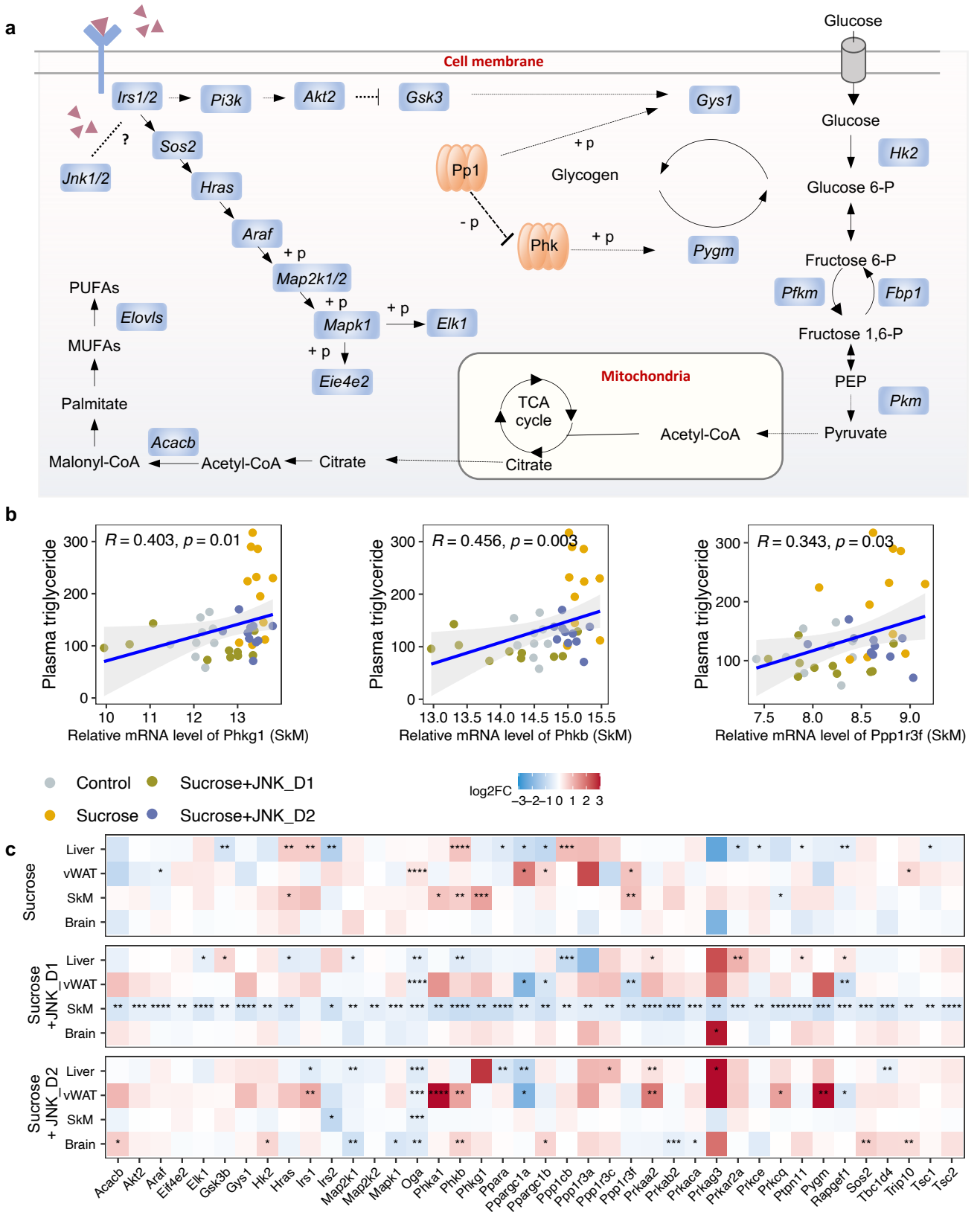

Figure 6. Inter-tissue network analysis reveals JNK-in-5A inhibition associated mechanism

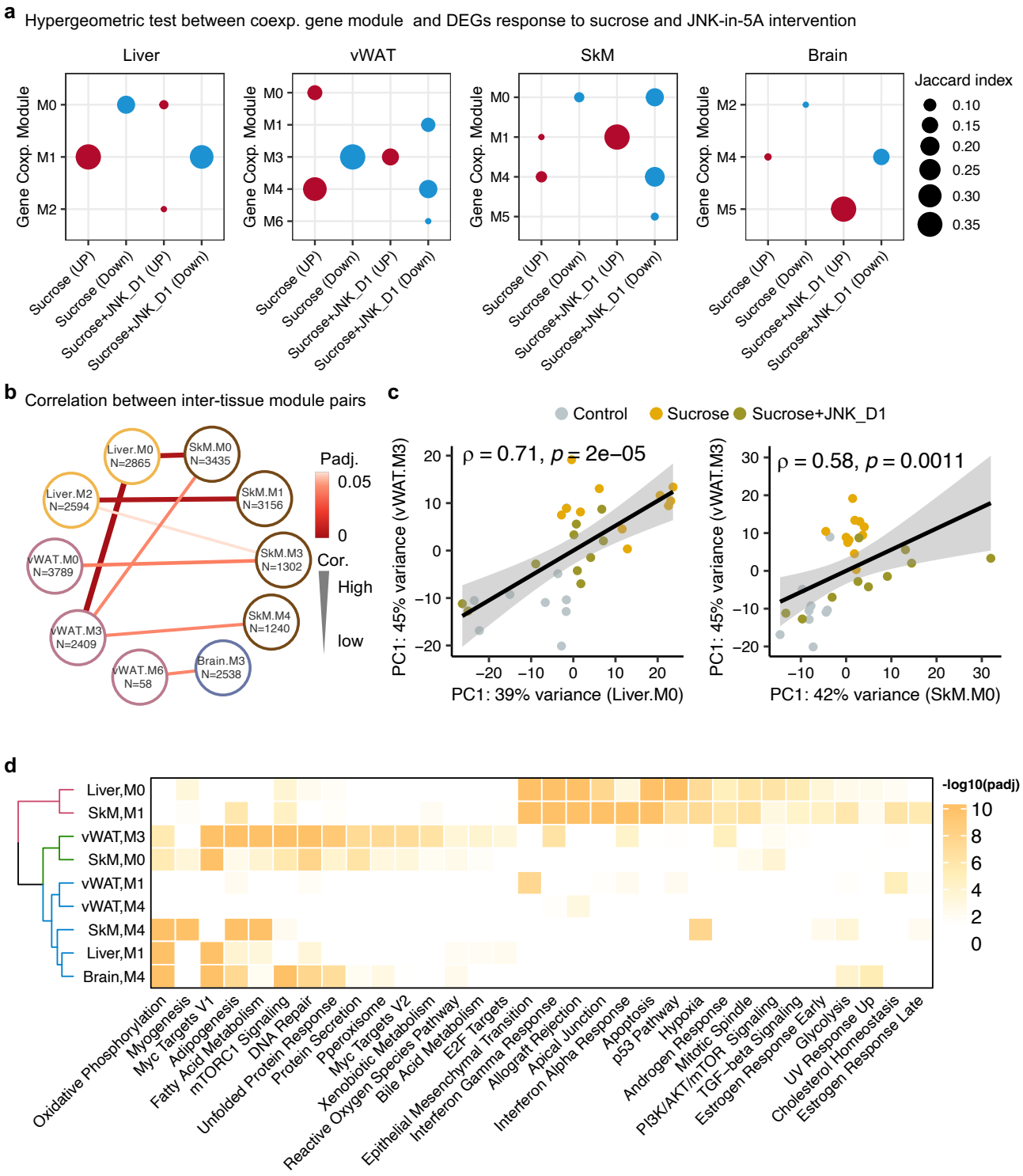

Figure 7. Metabolic modelling highlights the metabolic reprogramming upon JNK-in-5A inhibition

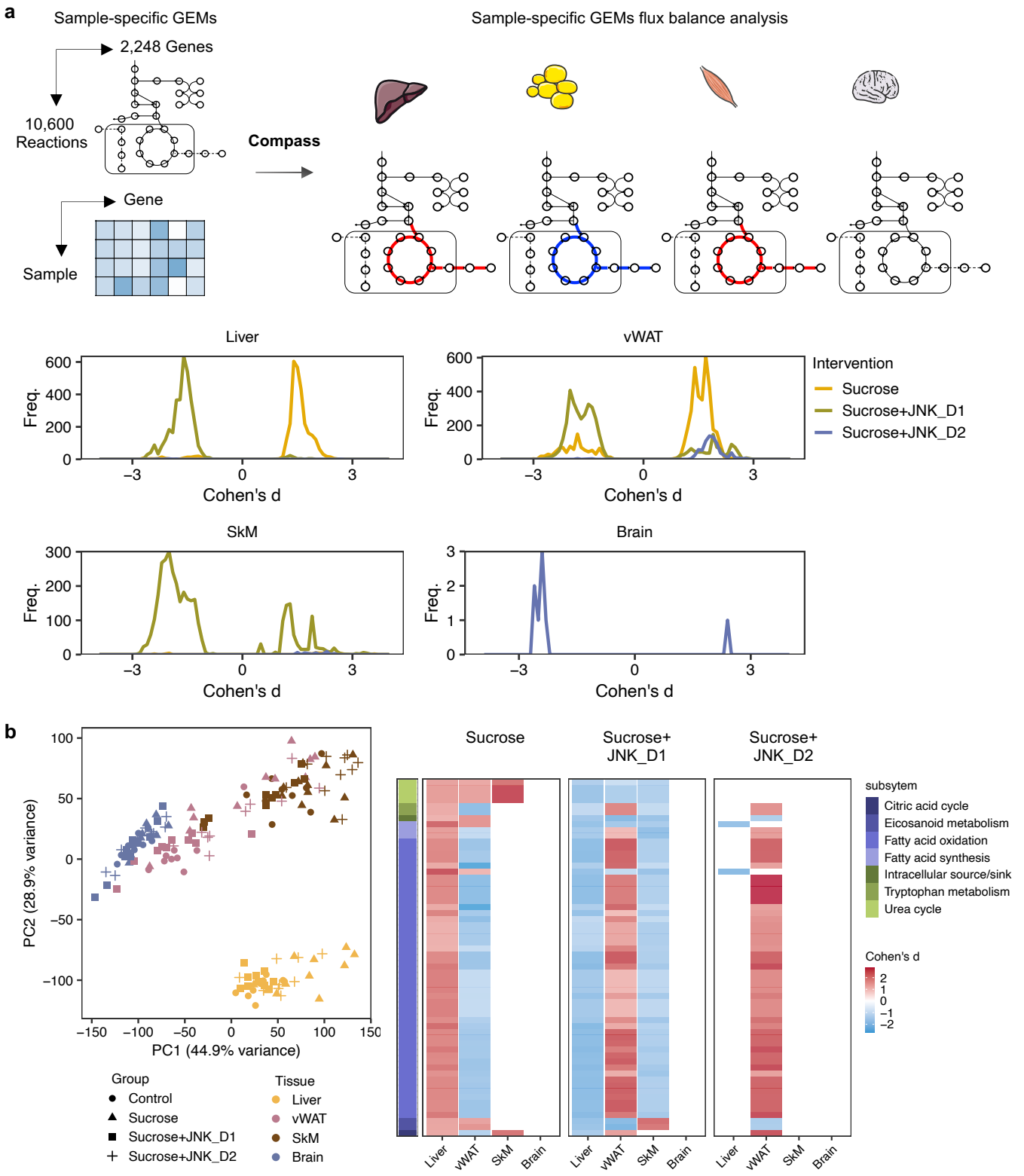

Figure S1

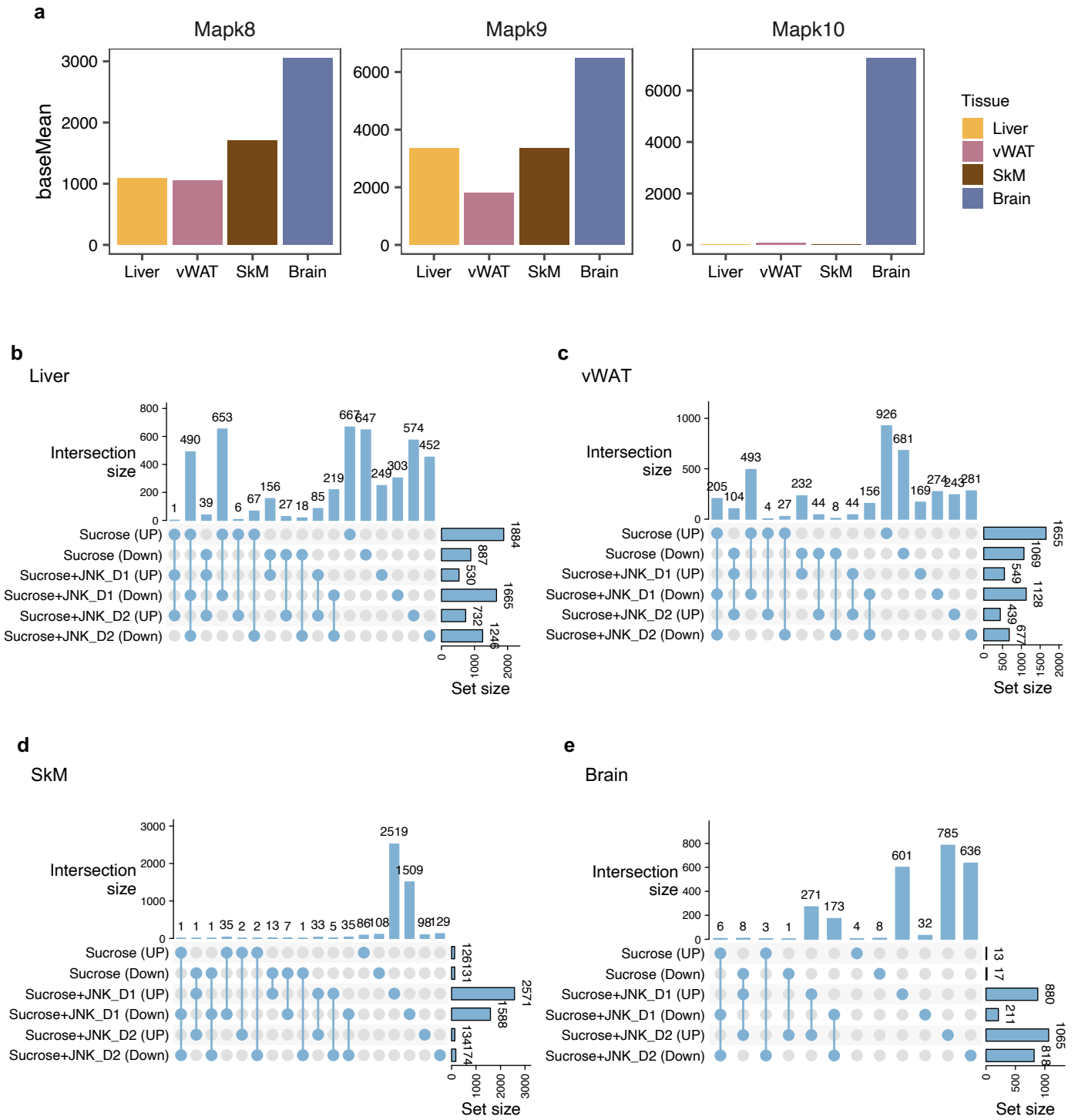
a
Mapk8
Mapk9
Mapk10
baseMean
Liver
vWAT
SkM
Brain
Tissue
Liver
vWAT
SkM
Brain
b
Liver
Intersection size
Sucrose (UP)
Sucrose (Down)
Sucrose+JNK_D1 (UP)
Sucrose+JNK_D1 (Down)
Sucrose+JNK_D2 (UP)
Sucrose+JNK_D2 (Down)
Set size
c
vWAT
Intersection size
Set size
d
SkM
Intersection size
Set size
e
Brain
Intersection size
Set size

Figure S2. Top-10 enriched gene signatures related to sucrose intake and sucrose+JNK_D1 administration

a

Liver tissue

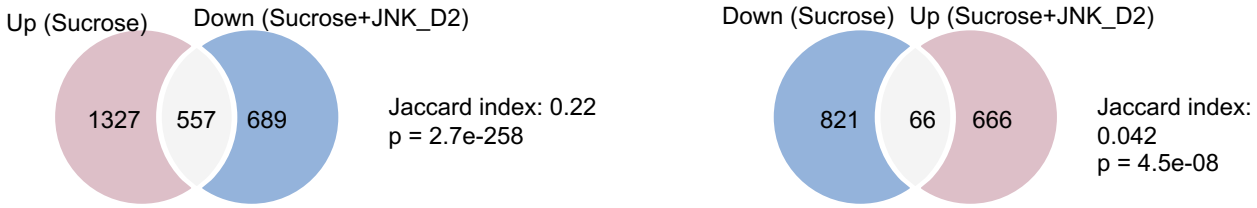

b

vWAT tissue

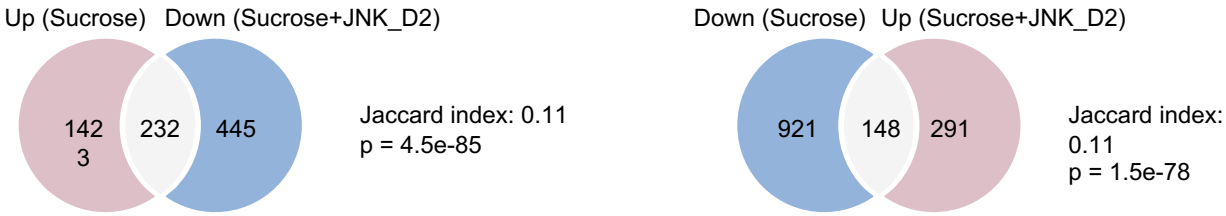

c

Liver tissue

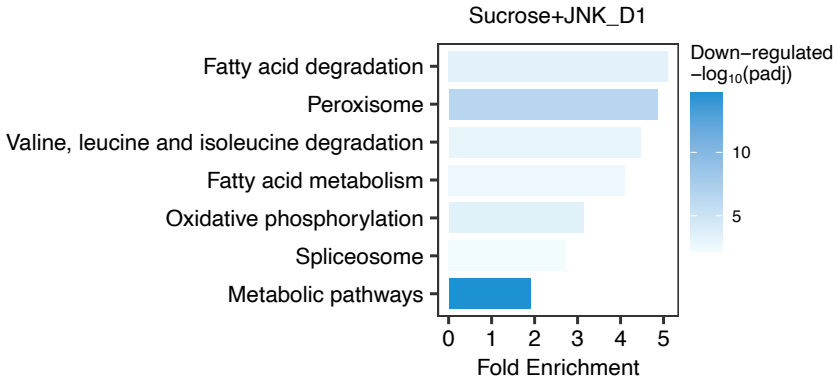

d

vWAT tissue

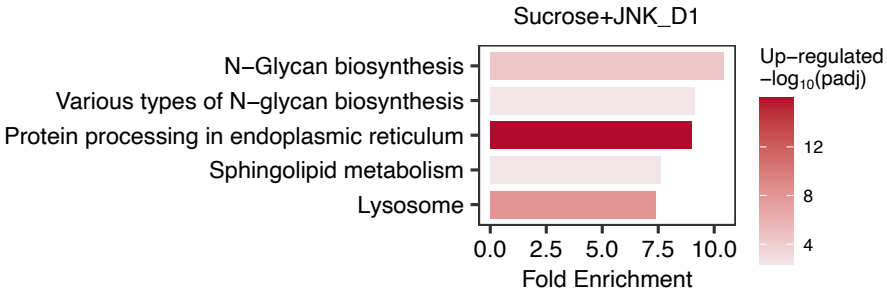

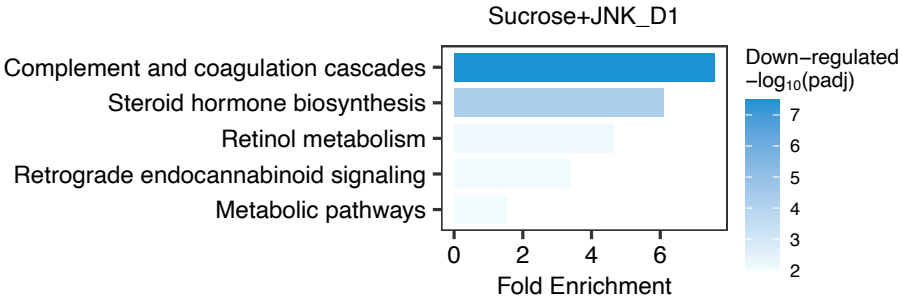

Figure S3. relative changes of genes involved in fatty acid metabolism, after JNK-in-5A treatment

A. Fatty acid metabolism
B. Fatty acid degradation
C. Fatty acid elongation
D. Fatty acid biosynthesis
E. Biosynthesis of unsaturated fatty acids

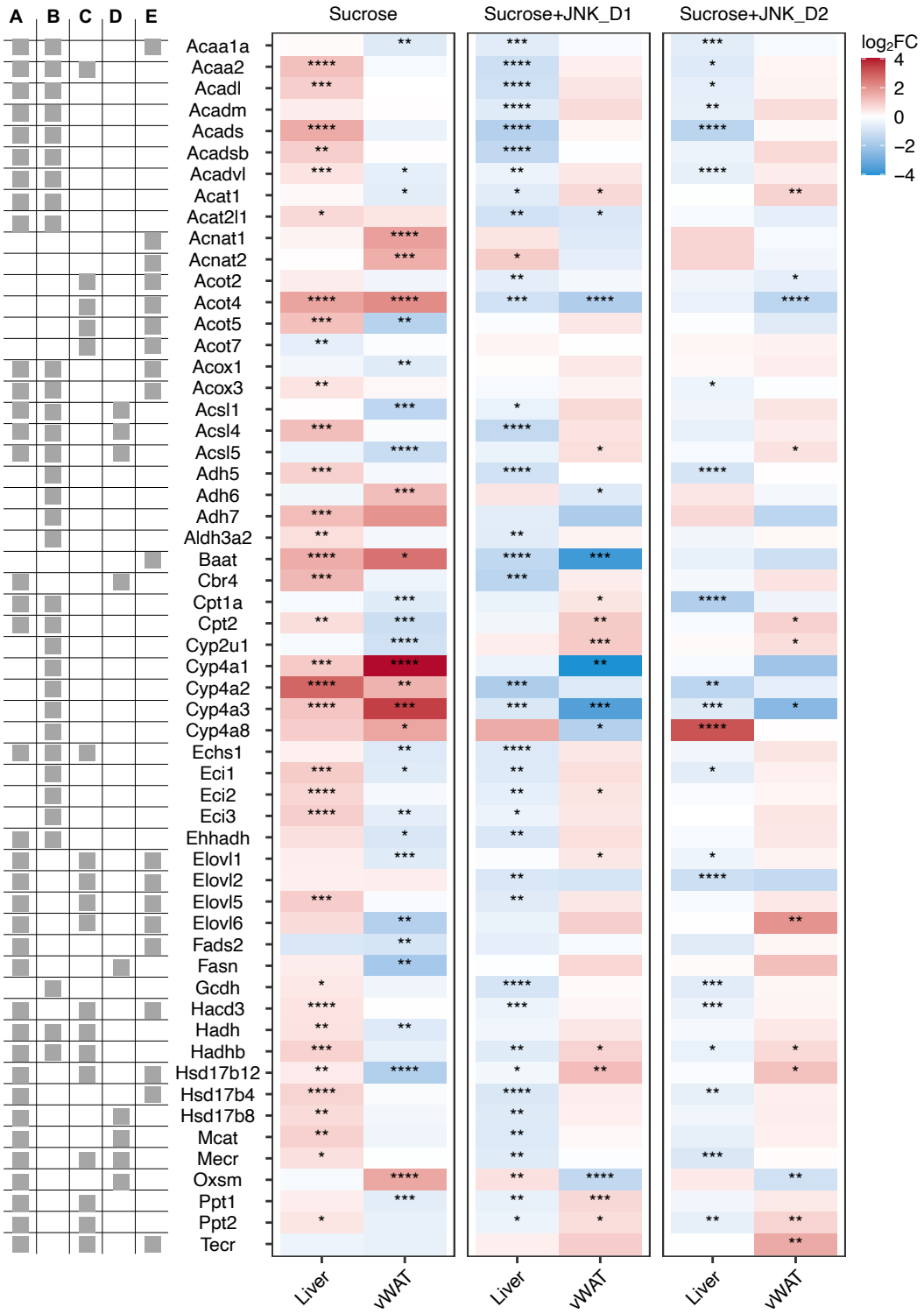

Figure S4. tissue-specific fatty acid (FA) uptake-related genes , after JNK-in-5A treatment

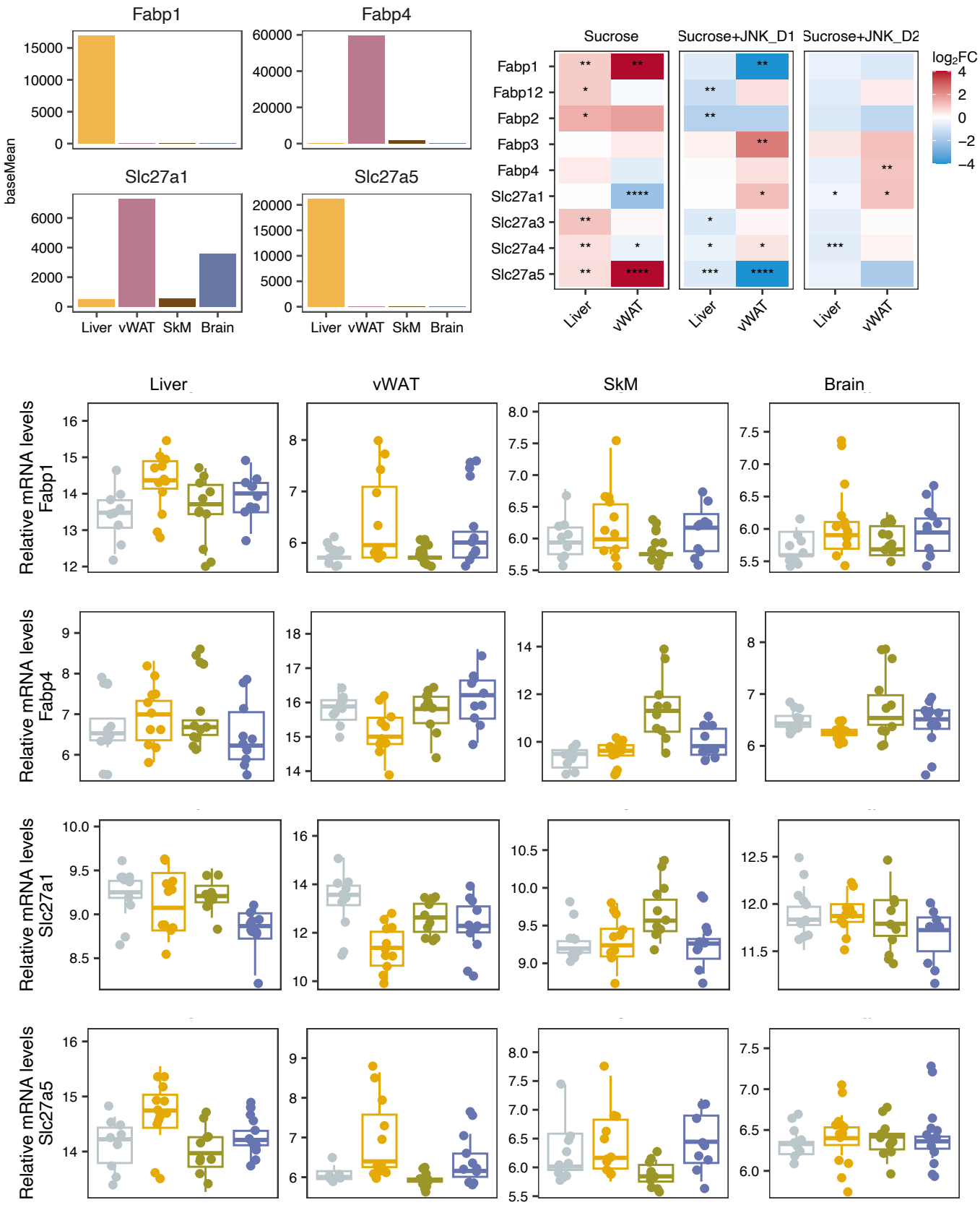

Figure S5. tissue-specific ROS-related genes , after JNK-in-5A treatment

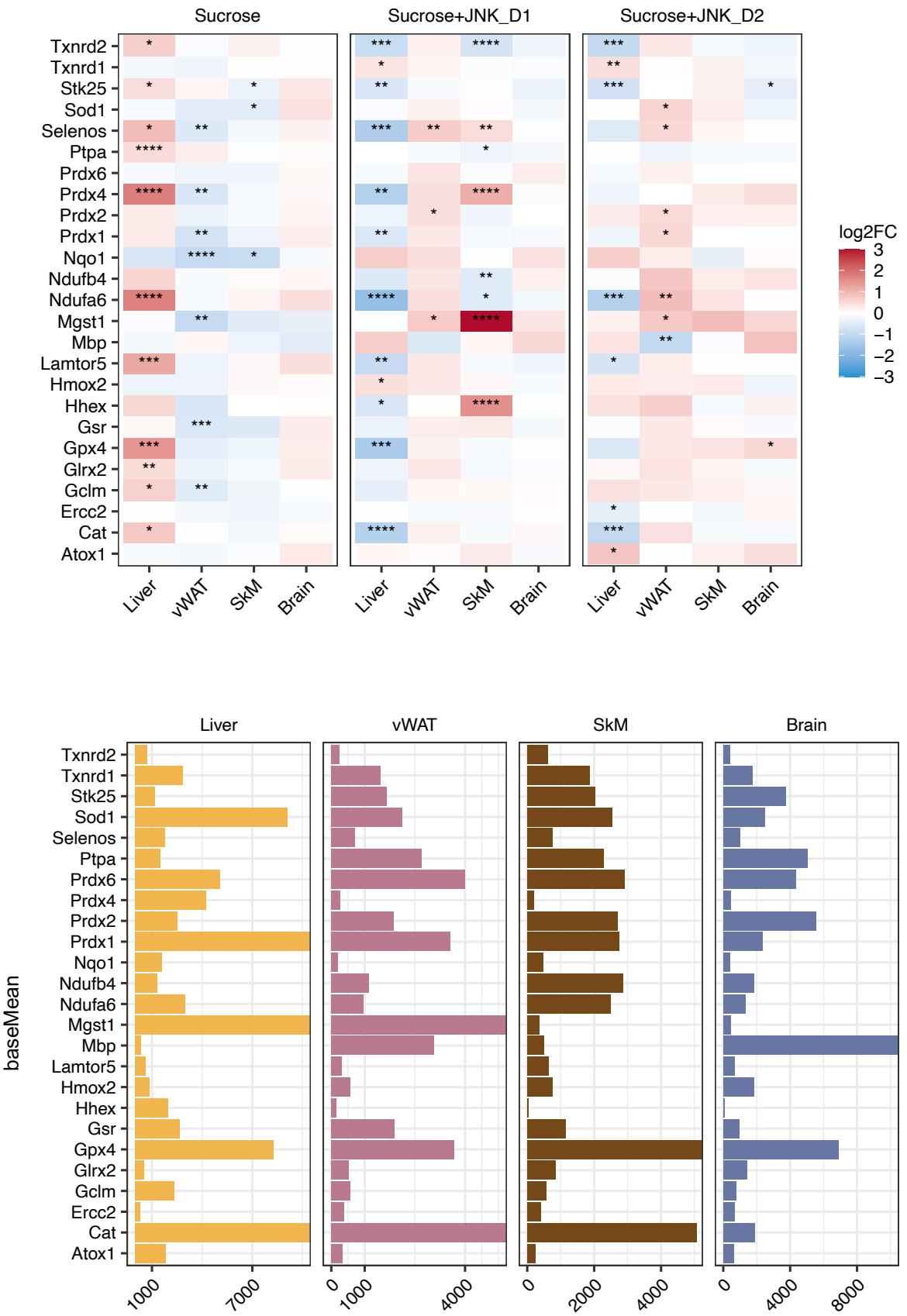

Figure S6. Skeletal muscle response to sucrose intake and sucrose+JNK_D2 administration

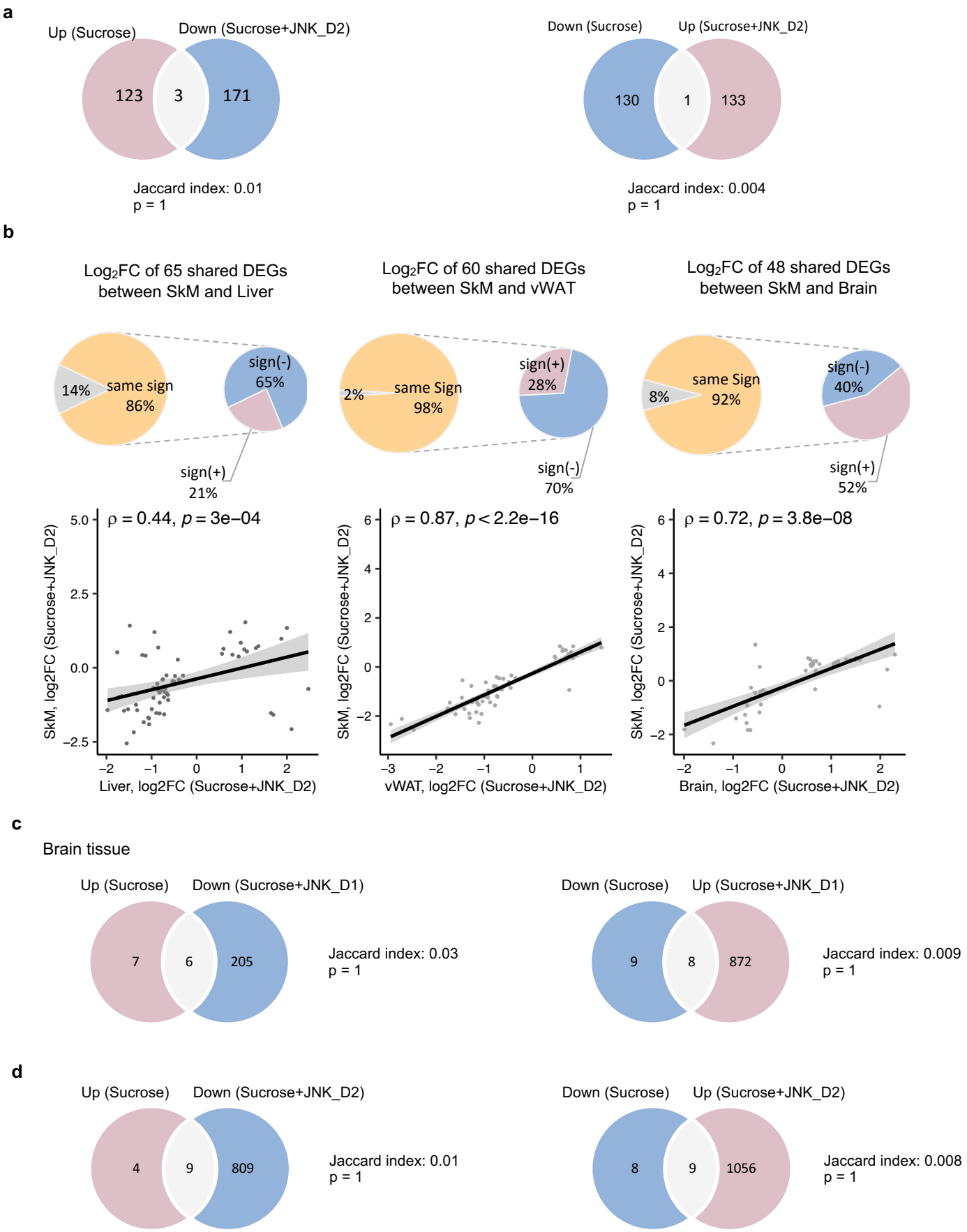

Figure S7. Tissue-specific and inter-tissue co-expression module analysis

a

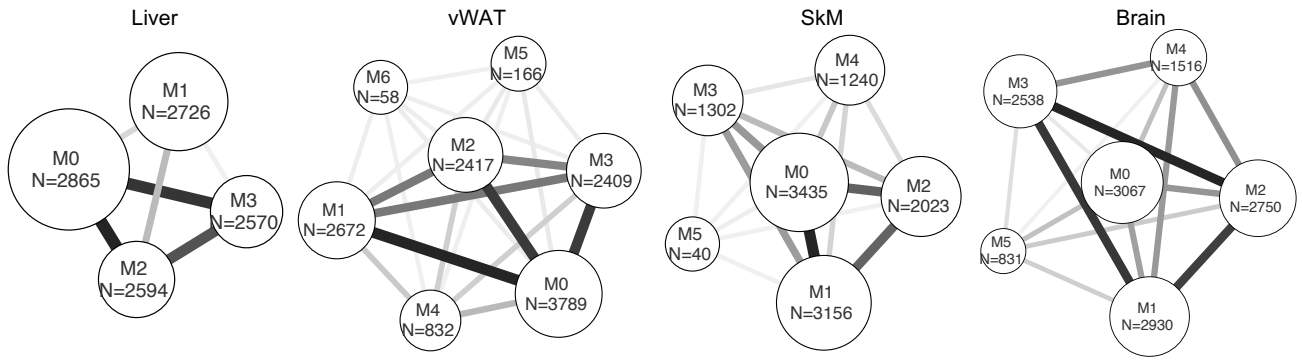

b

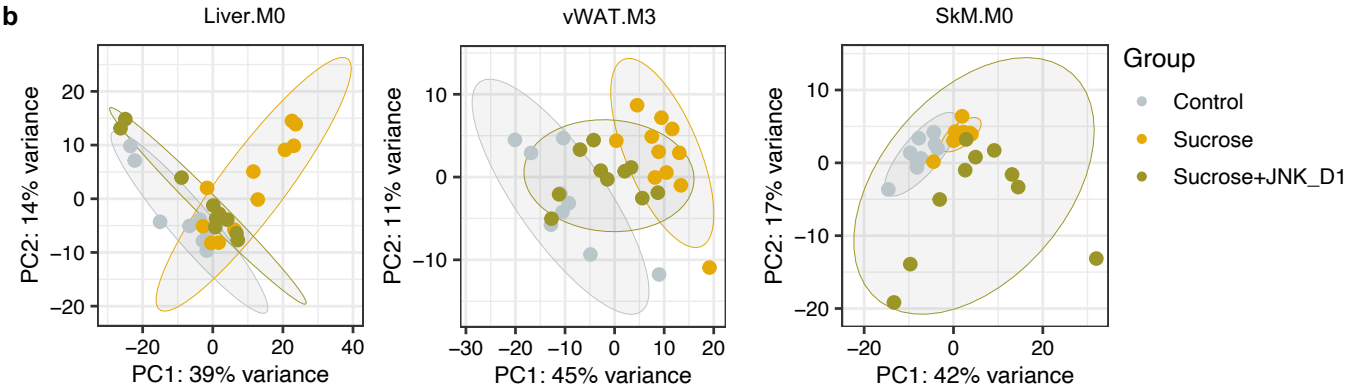

c
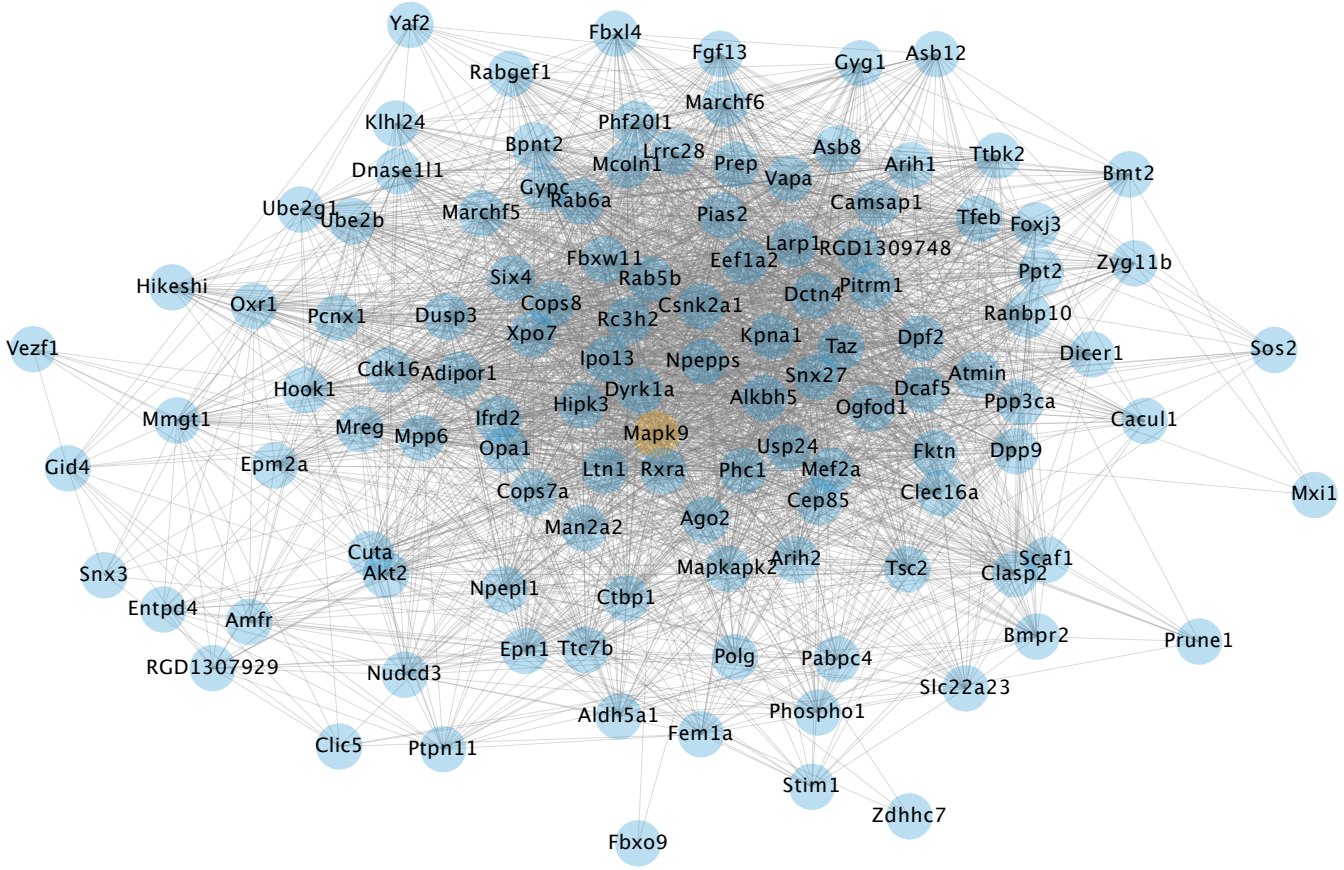
Module neighbors of Mapk9 in SkM.M0